Metabolic adaptation supports enhanced macrophage efferocytosis in limited-oxygen environments

Novel metabolic adaptation promotes enhanced macrophage efferocytosis under a limited-oxygen environment

Ya-Ting Wang[1], Alissa Trzeciak[1], Waleska Saitz Rojas[1], Pedro Saavedra[1], Yan-Ting Chen[2], Rachel Chirayil[3,4], Jon Iker Etchegaray[5], Christopher D. Lucas[6,7], Daniel Puleston[8], Kayvan R. Keshari[3,4], Justin S. A. Perry[1,2,9,^].

[1]Immunology Program, Memorial Sloan Kettering Cancer Center, New York, NY, United States.
[2]Louis V. Gerstner Jr. Graduate School of Biomedical Sciences, Memorial Sloan Kettering Cancer Center, New York, NY, USA.
[3]Department of Radiology, Memorial Sloan Kettering Cancer Center, New York, NY, USA.
[4]Molecular Pharmacology Program, Memorial Sloan Kettering Cancer Center, New York, NY, USA.
[5]Department of Microbiology, Immunology, and Cancer Biology, University of Virginia, Charlottesville, VA, USA.
[6]University of Edinburgh Centre for Inflammation Research, Queen's Medical Research Institute, Edinburgh BioQuarter, UK.
[7]Institute for Regeneration and Repair, Edinburgh BioQuarter, UK.
[8]Bloomberg-Kimmel Institute of Cancer Immunotherapy, Sidney Kimmel Comprehensive Cancer Center, Johns Hopkins University, Baltimore, MD, USA.
[9]Department of Immunology and Microbial Pathogenesis, Weill Cornell Medical College, New York, NY, USA.
^Corresponding author: perryj@mskcc.org

Summary

Apoptotic cell clearance (efferocytosis), a process essential for organismal homeostasis, is performed by phagocytes that inhabit harsh tissue environments, including physiologic hypoxia. Here, we find macrophages, the predominant tissue-resident phagocyte, display enhanced efferocytosis under chronic hypoxia, characterized by increased internalization and accelerated degradation of apoptotic cells. Analysis of transcriptional and translational programs revealed that macrophages under chronic hypoxia induce two distinct states. The first, 'primed', state consists of concomitant induction of transcriptional and translational programs broadly associated with metabolism in naïve macrophages that persist during efferocytosis. The second, 'poised', state consists of transcription, but not translation, of phagocyte function programs in naïve macrophages that are subsequently translated during efferocytosis. We discovered that one such primed state consists of the efficient flux of glucose into a noncanonical pentose phosphate pathway (PPP) loop, whereby PPP-derived intermediates cycle back through the PPP to enhance production of NADPH. Mechanistically, we found that PPP activity directly supports enhanced efferocytosis activity under chronic hypoxia while simultaneously maintaining redox homeostasis. Thus, macrophages adapt to chronic hypoxia by adopting states that both support cell fitness and ensure ability to rapidly and safely perform essential homeostatic functions.

Highlights

- Macrophages under chronic hypoxia enhance uptake and degradation of apoptotic cells
- Chronic hypoxia induces both primed and poised states in macrophages
- A noncanonical PPP loop is a unique primed state induced in macrophages
- This PPP loop both supports enhanced efferocytosis and maintains redox homeostasis

Introduction

Efferocytosis, the phagocytic clearance of apoptotic cells, is indispensable for organismal homeostasis (Boada-Romero et al., 2020; Doran et al., 2020; Rothlin et al., 2020). Efferocytosis likely occurs in all major tissues and organs, ensuring that disparate processes such as barrier epithelial cell recycling, removal of spent neutrophils and red blood cells, elimination of apoptotic neurons, and clearance of negatively-selected thymocytes (Elliott and Ravichandran, 2016; Henson, 2017; Morioka et al., 2019). These clearance processes are performed by various types of phagocytes, especially by tissue-resident macrophages (TRMs; (Penberthy et al., 2018; Zago et al., 2021)). At homeostasis, each tissue exhibits a substantial rate of cellular turnover, collectively amounting to ~1-2% body mass each day (Sender and Milo, 2021). As the body's main professional phagocyte, TRMs shoulder the brunt of this massive burden (Trzeciak et al., 2021).

TRMs are generally long-lived cells that seed a tissue early during development and often reside in a tissue throughout the organism's lifespan (Amit et al., 2016; Guilliams and Svedberg, 2021; Guilliams et al., 2020; Okabe and Medzhitov, 2016). It is now clear that TRMs adapt to their unique and often harsh tissue environment to perform their core functions (Amit et al., 2016; Blériot et al., 2020; Guilliams et al., 2020), including residing in tissues with a relative dearth of oxygen availability and exposure to tissue-specific debris and metabolites. For instance, the tissues that feature the most cell turnover (bone marrow, spleen, thymus; (Breed et al., 2019; Sender and Milo, 2021; Stritesky et al., 2013)) are also tissues with the lowest oxygen availability (Carreau et al., 2011; Norris et al., 2019; Trayhurn, 2019). TRMs, then, must both adapt to the tissue environment in which they reside and cope with the continuous influx of internalized biological material. Recent work has illustrated mechanisms by which phagocytes sense and respond to internalized apoptotic cells (Morioka et al., 2018; Perry et al., 2019; Wang et al., 2017; Yurdagul et al., 2020; Zhang et al., 2019), however, how tissue environment factors, such as oxygen availability, inform the ability to perform efferocytosis remains unknown.

Through our investigation of efferocytosis in physiologic hypoxia, we made the striking discovery that exposure to chronic hypoxia, similar to that experienced by several TRM

populations, resulted in increased internalization and accelerated degradation of apoptotic cells. We found that chronic exposure to hypoxia induced two distinct but complimentary states. One state, which we term ‘primed’, generally consists of simultaneous transcriptional and translational induction or suppression of metabolic programs in naïve macrophages that remain induced or suppressed during efferocytosis. The other state, which we term ‘poised’, generally consists of transcription, without concomitant translation, of phagocytic functional programs in naïve macrophages that are instead translated during efferocytosis. Subsequent exploration of primed state metabolic programs revealed that macrophages exposed to chronic hypoxia switch to the efficient utilization of glucose to generate NADPH via a noncanonical pentose phosphate pathway (PPP) loop that features recycling of PPP-derived intermediates back through the oxidative PPP. The PPP-dependent generation of NADPH prior to efferocytosis served to both support enhanced internalization and degradation of apoptotic cells via phagolysosomal maturation and protect phagocytes from runaway oxidative stress. These studies reveal that macrophages adapt to chronic hypoxia by acquiring distinct states that simultaneously support cell fitness and ensure the ability to perform critical homeostatic functions, such as efferocytosis.

Results

Efferocytosis is enhanced under prolonged ('chronic') hypoxia

Professional phagocytes, such as tissue-resident macrophages or macrophages in tumors, often reside for long periods of time in environments with extremely low oxygen (hypoxia; (Blériot et al., 2020; Guilliams et al., 2020)). Despite this relative dearth of oxygen, phagocytes must clear millions of apoptotic cells, a homeostatic process known as 'efferocytosis'. To address the effect of prolonged ('chronic') hypoxia on efferocytosis, we optimized a system and protocols to continually manipulate and culture primary professional phagocytes (macrophages) in low (1%) oxygen. Strikingly, chronic hypoxia-conditioned macrophages engulfed significantly more apoptotic cells than both macrophages cultured under 'standard' oxygen levels (21%) and macrophages exposed to 'acute' (3h) hypoxia (**Figure 1A**). Chronic hypoxia-conditioned macrophages engulfed significantly more apoptotic cells irrespective of the size of the target cell, the type of target cell, the method of cell death induction, the transformation status of the target cell, or the metastatic potential of the target cell (**Figure 1B**; Figure S1A-D). Furthermore, macrophages engulfed significantly more apoptotic cells regardless of whether they were differentiated in standard oxygen conditions or under hypoxia (**Figure 1C**).

Professional phagocytes are often responsible for engulfment of apoptotic cells in quick succession, a phenomenon known as 'continual efferocytosis', which protects against the manifestation of inflammatory disease, such as atherosclerosis (Park et al., 2011; Viaud et al., 2018; Wang et al., 2017; Yurdagul et al., 2020). Interestingly, chronic hypoxia-conditioned macrophages also performed significantly higher levels of continual efferocytosis (**Figure 1D**). Despite the increased proportion of macrophages engulfing more apoptotic cells on a population level, our flow cytometric analysis of the geometric mean fluorescence intensity of apoptotic cell uptake (a surrogate of uptake events per cell) was similar between conditions (Figure S1E), suggesting that either 1) individual macrophages do not take up more corpses, or 2) chronic hypoxia-conditioned macrophages engulf more apoptotic cells and digest engulfed apoptotic cells quicker on a per cell basis. To test these hypotheses, we performed time-lapse confocal microscopy of macrophages conditioned in standard oxygen or under chronic hypoxia.

Indeed, chronic hypoxia-conditioned macrophages not only engulfed significantly more apoptotic cells on a per cell basis (~60% engulfed 3 or more corpses per cell compared to 25% of macrophages cultured in standard oxygen) but also degraded engulfed apoptotic cells significantly faster (**Figure 1E and 1F**).

Several tissue-resident macrophage populations reside under physiological hypoxia. For instance, bone marrow-resident macrophages and macrophage subsets in the spleen chronically experience oxygen levels as low as ~1% (Norris et al., 2019). To test the physiological relevance of low oxygen conditioning on efferocytosis, we isolated macrophages from either the bone marrow or spleen and seeded them in either standard or 1% oxygen (**Figure 1G and 1H**). Consistent with our in vitro conditioning studies, we found that both bone marrow and splenic macrophages exhibited enhanced efferocytosis in the presence of 1% oxygen compared to standard oxygen (**Figure 1G and 1H**; Figure S1F). Collectively, our data suggest that professional phagocytes adapt to prolonged hypoxia to better engulf and digest potentially dangerous apoptotic cells.

Characterization of macrophage adaptation to chronic hypoxia

Cells are known to respond to acute hypoxia by stabilizing the hypoxia-inducible factor 1 subunit alpha or 2 alpha (HIF-1α and HIF-2α; (Lee et al., 2020)). Previous work remains controversial on the importance of HIF proteins for macrophage function in both standard oxygen and acute hypoxia (Acosta-Iborra et al., 2009; Anand et al., 2007; Dehn et al., 2016; Lin et al., 2018; Luo et al., 2016; Marsch et al., 2014). Contrarily, chronic hypoxia-conditioned macrophages significantly downregulate both HIF proteins (Figure S1G and S1H) suggesting that macrophages adapt to prolonged low oxygen by uncoupling from HIF signaling. This finding is consistent with recent work demonstrating that transformed cells (e.g., K562 cells) adapt to chronic hypoxia independent of HIF signaling (Jain et al., 2020). To investigate how macrophages adapt to chronic hypoxia, we performed RNA sequencing (RNAseq) of primary macrophages cultured in standard oxygen (21%), exposed to acute hypoxia (1% for 3h), and exposed to prolonged hypoxia (1% for 7d; **Figure 2A**). Analysis of chronic hypoxia-conditioned macrophages revealed several differentially expressed transcriptional programs (**Figure 2B**). For

instance, we observed significant downregulation of lipid and mitochondrial metabolism programs and upregulation of carbohydrate metabolism and hypoxia-responsive programs (**Figure 2B**), broadly consistent with a previous study of cancerous cells cultured under chronic hypoxia (Jain et al., 2020). Importantly, we observed several programs not previously associated with hypoxia generally, and chronic hypoxia specifically. For instance, we observed downregulation of metabolic programs (amino acid metabolism, oxidative stress/redox biology, insulin signaling), cell biological processes (endocytosis, mitochondrial biology, autophagy, pro-apoptotic signaling, exocytosis, vesicular transport), immune cell function (pro-inflammatory processes, antigen presentation), ion transport, and calcium homeostasis (**Figure 2B**; Figure S2A and S2B). On the other hand, we observed upregulation of key homeostatic macrophage function programs (phagocytosis, anti-inflammatory processes, wound healing, ECM Biology, angiogenesis), cell biological processes (lysosome biology, ER Stress/UPR, actin/cytoskeleton, cell adhesion, cell migration, anti-apoptotic signaling), and putative pro-tumorigenic programs (**Figure 2B**; Figure S2A and S2B). Although the majority of the chronic hypoxia-specific program was induced only after prolonged hypoxia, a fraction of the program was modestly, albeit non-significantly, induced in response to acute hypoxia (Chronic vs. Standard Only; **Figure 2C**). Because these genes continue to significantly increase after prolonged hypoxia, we consider them as part of the chronic hypoxia-induced program.

In parallel, we performed proteomic analysis of chronic hypoxia-conditioned macrophages. Our analysis revealed several differentially regulated programs that overlap with programs identified via RNAseq, especially programs involved in cellular metabolism (e.g., upregulation of carbohydrate metabolism, downregulation of lipid and mitochondrial metabolism; **Figure 2D**). We also observed upregulation of programs involved in nucleotide and nitrogen metabolism, and downregulation of a program involved in nitrogen catabolism. We subsequently validated representative targets fitting into one of three criteria: 1) Arginase 1 (ARG1, gene symbol *Arg1*), a target that was upregulated in both RNAseq and proteomics analysis, 2) transferrin receptor protein 1 (CD71, gene symbol *Tfrc*), a target that was downregulated in both RNAseq and proteomics analysis, and 3) 4-1BB (CD137, gene symbol *Tnfrs9*), a target that was upregulated in RNAseq but not detected via proteomics (**Figure 2E**).

Taken together, these data indicate that macrophages induce unique transcriptional and translational programs in response to chronic hypoxia and suggest that these adaptations support essential macrophage function under limiting oxygen environments.

Chronic hypoxia induces states both primed and poised for efferocytosis

Beyond the differentially-regulated genes that we failed to detect signal for in our proteomics analysis, we also made the striking observation that a plurality of genes significantly differentially regulated by chronic hypoxia are detected but remain unchanged at the protein level (Figure S3A). One hypothesis is that macrophages in specific environments, such as a tissue with low oxygen, accumulate function-specific mRNAs that allow for rapid protein synthesis in response to performing a canonical function. To test this, we used a strategy for performing mass spectrometry analysis of proteins in efferocytotic macrophages while excluding contaminating peptides from engulfed apoptotic cells. Specifically, we labeled live target cells with ^{13}C-lysine for >7 generations to stable isotope-label amino acids prior to induction of apoptosis and co-culture with conditioned macrophages (diagram in **Figure 3A**; global analyses in Figure S3B). Analysis of the core chronic hypoxia-induced transcriptional program revealed two distinct patterns of protein expression dynamics. First, we observed transcriptional programs that were also significantly differentially expressed at the protein level in resting macrophages, which typically remained significantly increased/decreased (or increased/decreased further) in efferocytotic macrophages ('Primed' Programs in **Figure 3A,** PFKL/*Pfkl* as a representative example in **Figure 3B**). This cluster consisted primarily of cellular metabolism programs, such as carbohydrate metabolism, lipid metabolism, and mitochondrial metabolism. Second, and far more surprisingly, we observed transcriptional programs that were not differentially expressed at the protein level in resting macrophages but were significantly differentially regulated in efferocytotic macrophages ('Poised' Programs in **Figure 3A**, PLOD1/*Plod1* as a representative example in **Figure 3B**). This cluster consisted primarily of macrophage function programs, including phagocytosis, ECM biology, and cell adhesion. Furthermore, many of these proteins were also differentially regulated at the protein level in efferocytotic macrophages cultured in standard oxygen (e.g., PLOD1 in **Figure 3B**), consistent

with the notion that these programs are generally important for core macrophage function. Thus, chronic hypoxia induces two distinct states in macrophages. The first state responds immediately by coupling transcription and translation to adapt to the local environment and prime resting macrophages for efferocytosis. The second state features transcriptional changes without commensurate protein translation in resting macrophages, instead poising resting macrophages with function-specific transcripts that are subsequently translated *during* efferocytosis.

Mapping the metabolic pathways unique to chronic hypoxia-conditioned macrophages

As part of our analysis of transcriptional programs in chronic hypoxia-conditioned macrophages, we performed a network analysis of the differentially regulated metabolic programs in 'primed' macrophages (**Figure 4A**, Figure S4A). Our analysis revealed that the broader metabolic programs clustered into specific metabolic pathways and processes. For instance, carbohydrate metabolism clustered into three categories: upregulation of gluconeogenesis/ glucose transport, downregulation of one carbon/aldehyde metabolism, and mixed regulation of the pentose phosphate pathway (PPP; **Figure 4A**). Given the highly coordinated regulation of specific metabolic pathways and processes in 'primed' macrophages, we explored further macrophage metabolism under chronic hypoxia. Consistent with our RNAseq and proteomics analyses, we observed significant differences in glucose uptake by macrophages conditioned in hypoxia (**Figure 4B**). However, contrary to our expectations, we observed (via enzymatic analysis) that chronic hypoxia-conditioned macrophages consume significantly less glucose from media than macrophages in standard oxygen (**Figure 4B**, left graph). Furthermore, chronic hypoxia-conditioned macrophages secrete less lactate (**Figure 4B**, right graph). Our data suggest that chronic hypoxia-conditioned macrophages perform less (an)aerobic glycolysis than macrophages cultured in standard oxygen.

Our findings suggesting that chronic hypoxia-conditioned macrophages consume and utilize less glucose was surprising given previous studies of cellular metabolism under hypoxia (Denko, 2008; Sadiku and Walmsley, 2019; Taylor and Colgan, 2017). To further elucidate the metabolic state of chronic hypoxia-conditioned macrophages, we performed untargeted

metabolomics analysis of macrophages cultured in standard oxygen, conditioned in hypoxia acutely, or conditioned chronically in hypoxia. Similar to our RNAseq analysis, chronic hypoxia-conditioned macrophages exhibited a different cellular metabolite profile than macrophages from either standard or acute hypoxia conditions (Figure S4B). Our analysis revealed significant upregulation of several pathways, including PPP, polyamine metabolism, and vitamin B6 metabolism (**Figure 4C and 4D**; Figure S4C). On the other hand, we observed downregulation of alanine/aspartate/glutamine metabolism, glycine/serine (one carbon) metabolism, and niacin/nicotinamide (vitamin B3) metabolism (**Figure 4C and 4D**; Figure S4C). We also observed decreased TCA cycle intermediates (Figure S4C), consistent with our observation that chronic hypoxia-conditioned macrophages downregulate a mitochondrial metabolism transcriptional program (Figure S4A). Analysis of individual metabolites revealed relative enrichment of key PPP intermediates and the upstream glycolysis intermediates glucose 6-phosphate, fructose 6-phosphate, and fructose 1,6-bisphosphate but downregulation of/no change in downstream glycolysis intermediates, including glyceraldehyde 3-phosphate and pyruvate (**Figure 4D**; Figure S4C). Thus, chronic hypoxia-conditioned macrophages induce or suppress distinct metabolic programs, in particular increased PPP activity despite decreased glucose uptake/lactate secretion.

Macrophages adapt to chronic hypoxia by co-opting a noncanonical pentose phosphate loop to ensure redox homeostasis

Beyond ATP generated during glycolysis, glucose also contributes to both redox homeostasis (e.g., NADPH generation) and nucleotide synthesis by shunting the glycolysis intermediate glucose 6-phosphate (G6P) into the pentose phosphate pathway (PPP; **Figure 5A**). Our finding that chronic hypoxia-conditioned macrophages consume less glucose, secrete less lactate, and accumulate fewer TCA cycle intermediates but significantly accumulate PPP intermediates suggests that macrophages may be utilizing glucose in an unconventional way. One possibility is that chronic hypoxia-conditioned macrophages accumulate PPP intermediates because of more efficient use of glucose for PPP, i.e., more G6P enters the PPP per molecule of glucose. To test this hypothesis, we performed 1,2-^{13}C-glucose tracing of standard oxygen- and

chronic hypoxia-conditioned macrophages. Tracing and LC-MS analysis using 1,2-^{13}C-glucose allowed us to determine the fraction and relative abundance of metabolic intermediates downstream of glucose, including glycolysis, PPP, and the re-synthesis of glycolysis intermediates via gluconeogenesis (**Figure 5A**; (Jang et al., 2018)). In chronic hypoxia-conditioned macrophages, we observed increased fractional enrichment and relative abundance of several intermediates that had cycled through the PPP (M+1 isotopologues, **Figure 5A**; Figure S5A), including fructose 6-phosphate (F6P), fructose 1,6-bisphosphate (FBP), and 3-phosphoglycerate (3PG). Additionally, chronic hypoxia-conditioned macrophages exhibited increased relative abundance of the committed PPP intermediate sedoheptulose 7-phosphate (S7P; Figure S5A). Contrarily, we observed decreased fractional enrichment and relative abundance of the terminal glycolysis intermediates phosphoenolpyruvate (PEP) and lactate as well as decreased contribution of glucose to the glucose-alanine and TCA cycles in chronic hypoxia-conditioned macrophages (Figure S5A). Consistent with our LC-MS analysis of cell pellets, we detected significantly less M+1 (via PPP) and M+2 (via glycolysis) lactate in conditioned media from chronic hypoxia-conditioned macrophages (using carbon nuclear magnetic resonance; **Figure 5B**), suggesting that chronic hypoxia-conditioned macrophages utilize less glucose for energy generation via glycolysis, instead efficiently shunting glucose into the PPP.

As part of our 1,2-^{13}C-glucose tracing studies, we observed the appearance of intermediates with ^{13}C labeling beyond the first and second position (**Figure 5C**; Figure S5B). For instance, we observed increased fractional enrichment and relative abundance of M+3, M+4, and M+5 isotopologues of G6P in chronic hypoxia-conditioned macrophages (**Figure 5C**; Figure S5B). The presence of these isotopologues could only arise if intermediates generated during glycolysis or PPP cycled back to G6P, through a process resembling gluconeogenesis in the liver (Hers and Hue, 1983). Unlike conventional gluconeogenesis, however, we did not detect newly synthesized glucose. Instead, together with G6P, we observe increased relative abundance of the glycolytic intermediates F6P (M+3, M+4), FBP (M+3, M+4), and 3PG (M+3; **Figure 5C**). Additionally, we observed increased relative abundance and fractional enrichment of M+3, M+4, and M+5 isotopologues of S7P (**Figure 5C**; Figure S5B). In parallel, we performed

uniformly-labeled (U)-^{13}C-glucose tracing of standard oxygen- and chronic hypoxia-conditioned macrophages to specifically test glucose carbon recycling and turnover (**Figure 5D**). Similar to our 1,2-^{13}C-glucose tracing studies, we observed less fractional enrichment and relative abundance of the glycolysis-generated M+3 lactate isotopologue in chronic hypoxia-conditioned macrophages (**Figure 5D**; Figure S5C). Furthermore, chronic hypoxia-conditioned macrophages exhibited increased fractional enrichment and relative abundance of the gluconeogenesis-generated M+3 G6P and F6P isotopologues (**Figure 5D**; Figure S5C) without appreciable gluconeogenesis-generated M+3 glucose (Figure S5C). Of the additional possible fates for glucose, chronic hypoxia-conditioned macrophages produced less alanine and decreased contribution to the TCA cycle, irrespective of route (via M+2 citrate or M+3 oxaloacetate, **Figure 5E**; Figure S5D and S5E). Finally, glucose that enters the PPP can provide the five-carbon nucleoside sugar necessary for *de novo* nucleotide synthesis. Surprisingly, we observed decreased *de novo* synthesis of both inosine monophosphate (IMP) and guanosine monophosphate (GMP; Figure S6F) in chronic hypoxia-conditioned macrophages, suggesting that the adaptation macrophages undergo in response to hypoxia includes a specific repurposing of glucose for the generation of NADPH.

Although the conventional PPP is thought to be important for inflammatory macrophage function, this often coincides with enhanced glycolysis, decreased G6P, and increased TCA cycle intermediates such as succinate and oxaloacetate (Artyomov and Van den Bossche, 2020; Makowski et al., 2020; Ryan and O'Neill, 2020). Contrarily, we observe increased PPP absent the other features present in inflammatory macrophages, suggesting that chronic hypoxia-conditioned macrophages co-opt an unconventional PPP. In support of this, we detected M+0 and M+2 sedoheptulose 1,7-bisphosphate (SBP) only in chronic hypoxia-conditioned macrophages (**Figure 5C**). SBP is an unusual metabolite, previously identified as a novel PPP intermediate in the liver (L-type PPP; (Cheng et al., 2019; Longenecker and Williams, 1980; Williams et al., 1985)). SBP is proposed to be synthesized via three different routes: 1) from dihydroxyacetone phosphate and erythrose 5-phosphate or 2) ribose 5-P via aldolase (e.g., ALDOA), and 3) from S7P via 6-phosphofructokinase (e.g., PFKL). We observed concomitant increases in mRNA and protein for aldolase (ALDOA and ALDOC) and 6-

phosphofructokinase (PFKL and PFKP) (**Figure 2**). Interestingly, a recent report found that SBP accumulates in the hepatoma Hep G2 line in response to oxidative stress (Cheng et al., 2019), suggesting that cells upregulate noncanonical PPP to cope with contexts that pose a danger to redox homeostasis. Indeed, chronic hypoxia-conditioned macrophages exhibited increased synthesis of NADPH and a decreased ratio of NADP+ to NADPH (**Figure 5F**, Figure S6A). Furthermore, macrophages exhibit lower lipid peroxidation and cellular oxidative stress (**Figure 5G**; Figure S6B), further supporting the notion that macrophages adapt to hypoxia by enhancing reductive potential and actively maintaining redox homeostasis.

Our RNAseq and proteomic analyses suggested that macrophages respond to chronic hypoxia by regulating mitochondrial metabolism and mitochondrial biology (e.g., mitochondrial quality control) programs (**Figure 2 and 4A**; Figure S2 and S3C), which are major contributors to the redox state of a cell (Muri and Kopf, 2020). Subsequent confocal microscopy and flow cytometric analysis of macrophages revealed decreased mitochondrial mass and increased mitochondrial fragmentation in chronic hypoxia-conditioned macrophages (Figure S6C-F), suggesting that macrophages limit mitochondrial processes that produce reactive species when exposed to chronic hypoxia. Additionally, chronic hypoxia-conditioned macrophages exhibited decreased mitochondrial superoxide levels (Figure S6G). As further evidence of decreased mitochondrial oxidative processes, we observed decreased total glutathione synthesis, reduced glutathione (GSH), and oxidized glutathione (GSSG) in chronic hypoxia-conditioned macrophages relative to standard oxygen-conditioned macrophages, albeit with a modest increase in the GSH/GSSG ratio (Figure S6H). Our finding of decreased glutathione synthesis mirrors our RNAseq results that chronic hypoxia-conditioned macrophages upregulated some oxidative stress/redox biology programs but decreased others (**Figure 2B**) including decreased glutamine metabolism and glutathione synthesis (Figure S4A). Collectively, our data indicate that macrophages adapt to chronic hypoxia by preferentially shunting glucose into a noncanonical pentose phosphate loop that enhances NADPH generation and suppresses cellular oxidative stress.

The noncanonical pentose phosphate loop supports continual efferocytosis via NADPH production and prevention of oxidative stress

To explore how induction of noncanonical pentose phosphate pathway (PPP) activity, a chronic hypoxia-induced 'priming' signal, directly affects efferocytosis, we co-opted multiple strategies to target the PPP specifically during efferocytosis (**Figure 6A**). First, we used the well-characterized noncompetitive inhibitor of glucose-6-phosphate dehydrogenase (G6PD), G6PDi-1, to block the NADPH-producing conversion of G6P to 6-phosphogluconolactone (6PGL) which resulted in decreased efferocytosis by chronic hypoxia-conditioned macrophages but not macrophages cultured in standard oxygen (**Figure 6B**, left bar graph). Second, we targeted 6-phosphogluconate dehydrogenase (6PGD), the enzyme responsible for the second NADPH-producing step that converts 6-phosphogluconate (6PG) into ribose 5-phosphate (R5P), using the specific small molecule inhibitor 6-aminonicotinamide (6-AN). Similar to G6PDi-1, inhibition of 6PGD resulted in significantly decreased efferocytosis in chronic hypoxia-conditioned macrophages (**Figure 6B**, center bar graph). Third, to test the contribution of gluconeogenesis to efferocytosis, we targeted fructose 1,6-bisphosphatase-1 (FBP1) activity using the selective inhibitor FBPi, which blocks the rate-limiting conversion of fructose 1,6-bisphosphate (FBP) to fructose 6-phosphate (F6P). Consistent with our tracing studies suggesting that PPP intermediates cycle back to G6P, we found that FBP1 inhibition led to decreased efferocytosis exclusively in chronic hypoxia-conditioned macrophages (**Figure 6B**, right bar graph). Collectively, our combination of approaches targeting components of the noncanonical PPP loop suggest that macrophages depend on this loop for efficient efferocytosis in low oxygen environments.

Considering our previous observation that chronic hypoxia-conditioned macrophages exhibit enhanced continual efferocytosis, we queried whether PPP activity is required for this enhancement. Targeting of 6PGD activity not only suppressed engulfment of the first corpse but also reduced engulfment of subsequent corpses (**Figure 6C**), suggesting that PPP activity is required for continual efferocytosis by chronic hypoxia-conditioned macrophages. Enhanced continual efferocytosis depends on a phagocytes ability to rapidly mature the phagolysosome and degrade apoptotic cells, as observed in chronic hypoxia-conditioned macrophages (**Figure**

1E and 1F). We subsequently tested whether perturbation of the PPP affects per cell engulfment and rate of apoptotic cell digestion. Time-lapse confocal microscopy revealed three key findings. First, inhibition of 6PGD activity resulted in fewer macrophages engulfing apoptotic cells, consistent with our population-level analysis of efferocytosis (**Figure 6D**). Second, we observed that macrophages engulf significantly fewer apoptotic cells on a per cell basis (6-AN-treated macrophages: ~80% engulfed 2 or fewer corpses per cell compared to 70% of untreated macrophages which engulfed 3 or more corpses per cell) when 6GPD activity was inhibited (**Figure 6D**, left bar graph). Finally, inhibition of 6PGD activity resulted in a slower rate of apoptotic cell degradation (**Figure 6D**, right bar graph), essentially reversing the benefit provided by chronic hypoxia 'priming'.

Phagolysosomal maturation and subsequent apoptotic cell degradation requires NADPH oxidase activity (Bagaitkar et al., 2018) but if not buffered against, can lead to excessive/runaway lysosomal acidification and oxidative stress (Mantegazza et al., 2008; Yvan-Charvet et al., 2010). NADPH, therefore, serves as both a substrate for reactive oxygen species production and an essential reducer of antioxidant molecules. NADPH is produced through three main pathways: the conversion of malate to pyruvate via malic enzyme 1 (ME1) activity, through conversion of isocitrate into alpha-ketoglutarate via isocitrate dehydrogenase 1 (IDH1) activity, and during the oxidative phase of the PPP. Macrophages under standard oxygen conditions produce minimal NADPH (**Figure 5F**; (Yvan-Charvet et al., 2010)) and possibly utilize one of the TCA cycle-related routes (ME1 or IDH1) to generate NADPH during efferocytosis *in vitro* as well as in macrophages localized to tissues with higher oxygen availability (Zhang et al., 2019). Consistent with our finding that chronic hypoxia-conditioned macrophages exhibit decreased glucose flux into the TCA cycle (**Figure 5E**) and increased flux into the PPP (**Figure 5A and 5C**), we observed concomitant PPP-dependent production of NADPH (**Figure 6E**). Although NADPH production remained abundant during efferocytosis by chronic hypoxia-conditioned macrophages (**Figure 6F**, compare solid red and purple bars), NADPH pools were further depleted in efferocytotic macrophages with perturbed 6PDG activity (**Figure 6F**, compare solid and striped purple bars).

Given the dependence on PPP for NADPH production in chronic hypoxia-conditioned macrophages, we subsequently sought to determine if PPP activity is required to maintain lysosomal homeostasis. In resting macrophages, inhibition of 6PDG activity resulted in a modest, albeit significant, increase in lysosomal acidity (**Figure 6G**, compare red bars). On the other hand, efferocytotic macrophages with perturbed 6PDG activity displayed significantly higher lysosomal acidity than untreated naïve and efferocytotic macrophages (**Figure 6G**, purple striped bar). Our observation that disruption of PPP activity alters basal and, to a greater extent, efferocytotic lysosomal acidity is consistent with previous work demonstrating that pharmacological targeting of NADPH oxidase activity results in increased lysosomal acidity in both resting and efferocytotic macrophages (Mantegazza et al., 2008). Lastly, we tested the hypothesis that disrupted PPP activity leads to increased oxidative stress in efferocytotic macrophages. Similar to our finding of increased lysosomal acidity, we observed that perturbation of 6PDG resulted in significantly increased lipid peroxidation (**Figure 6H**, purple striped bar) and cellular oxidative stress (**Figure 6I**, purple striped bar) in efferocytotic macrophages. Thus, our data suggest that PPP-mediated NADPH production protects efferocytotic macrophages from excessive lysosomal acidification and oxidative stress under settings of prolonged hypoxia.

Perturbation of the pentose phosphate pathway alters tumor-associated macrophage phenotype and impedes breast cancer progression

Oxygen levels very both across tissue types and within tissues, from relatively high (100 mmHg or ~13.5% O_2 in lung alveoli upon inspiration) to physiologic hypoxia (8 mmHg or ~1% O_2 in the bone marrow) (Carreau et al., 2011; Trayhurn, 2019). Interestingly, many solid cancers exhibit significantly lower oxygen levels than corresponding healthy tissues (Carreau et al., 2011). For instance, breast cancers (such as triple negative breast cancer) are characterized by a hypoxic microenvironment (10 mmHg or ~1.3% O_2) which is approximately 5-fold lower than healthy mammary tissue (52 mmHg or ~6.8% O_2) (Carreau et al., 2011). Breast cancer exhibits extensive cell death and high numbers of tumor-associated macrophages (TAMs), both of which indicate poor prognosis (Alexandrou et al., 2019; Bianchini et al., 2016; Medrek et al., 2012;

Mehanna et al., 2019; Yuan et al., 2014). Furthermore, previous studies suggest that efferocytosis is important for breast cancer development and progression in animal models (Cook et al., 2013; Stanford et al., 2014; Werfel et al., 2019). Thus, we tested whether pharmacological perturbation of PPP metabolism affected disease progression and TAM phenotype in an orthotopic breast cancer model. Treatment of mice bearing palpable tumors with the 6PGD inhibitor 6-AN resulted in both decreased tumor progression and smaller overall tumor size (**Figure 7A**; Figure S7A). The tumor microenvironment (TME) is dominated by pro-tumorigenic, pro-metastatic TAMs that exhibit a pro-resolving phenotype that is thought to be characterized by, among other factors, high CD11b expression, low/intermediate F4/80 expression, low MHC class II (MHCII) expression, and high Arginase 1 (Arg1) expression (CITES). Indeed, untreated orthotopic breast tumors exhibited a high frequency of CD11b^{high} F4/80^{int} TAMs (**Figure 7B**; Figure S7B). On the other hand, treatment of tumor-bearing mice with 6-AN resulted in a significant decrease in CD11b^{high} F4/80^{int} TAMs with a concomitant increase in CD11b^{high} F4/80^{high} TAMs (**Figure 7B**), which were previously identified in other tissues as pro-inflammatory (Hill et al., 2018; Lee et al., 2018; Schmid et al., 2018; Wang et al., 2011). Furthermore, we observed a significant increase in CD8+ T cells without significant changes in CD4+ T cells, Foxp3+ regulatory T cells, NK1.1+ NK cells, or CD19+ B cells (**Figure 7C**; Figure S7C), consistent with previous reports demonstrating that immune-mediated tumor regression depends on increased infiltration and activity of CD8+ T cells (Egelston et al., 2019; Huang et al., 2015).

Our initial analysis of TAMs from tumor-bearing mice suggested that 6-AN treatment was skewing macrophages from the canonically pro-tumorigenic, pro-resolving phenotype to a more inflammatory, anti-tumor phenotype. One hallmark of the pro-resolving macrophage phenotype is expression of the enzyme Arg1, known to be induced by both IL-4 and efferocytosis (Bosurgi et al., 2017) but was also identified as a 'primed' factor in chronic hypoxia-conditioned macrophages (**Figure 2E and 3A**). We observed a striking decrease in the frequency of Arg1 single-positive (Arg1+) cells across all myeloid subsets analyzed (**Figure 7D**). The decrease in Arg1+ cells was most pronounced in the putative pro-resolving CD11b^{high} F4/80^{int} TAMs, suggesting that pre-existing TAMs were altered in response to 6-AN treatment.

Additionally, the loss of Arg1+ myeloid cells was accompanied by significant increases in MHCII single positive (MHCII+) and MHCII+ Arg1+ myeloid cells (**Figure 7D**). As previously reported, MHCII expression in myeloid cells is associated with a canonical pro-inflammatory phenotype and observed in the context of successful anti-tumor immunity (Wang et al., 2011). Similar to Arg1, the most dramatic change was the appearance of MHCII+ cells in the CD11b^{high} F4/80^{int} TAM fraction. Surprisingly, however, we also observed a significant increase in MHCII+ Arg1+ cells in both CD11b^{high} F4/80^{int} TAMs and CD11b^{high} F4/80^{high} TAMs (**Figure 7D**). These cells may denote a transitional population between Arg1+ and MHCII+ myeloid cells, such as cells moving from regions of lower to higher oxygen or in the case of PPP metabolism perturbation, myeloid cells shifting metabolic dependence. Thus, pharmacological targeting of PPP metabolism slows progression and skews the TAM phenotype from pro-resolving to pro-inflammatory, including decreased frequency of TAMs expressing the chronic hypoxia-induced priming factor Arg1, in an orthotopic model of breast cancer.

Finally, we sought to determine if breast tumors treated with 6-AN exhibit altered apoptotic cell clearance similar to the decreased clearance observed *in vitro*. Given that efferocytosis *in vivo* is rapid and efficient, most tissues, including the parenchyma of solid cancers (as opposed to vascularized necrotic core), exhibit only rare secondary apoptotic/early necrotic cells (Elliott and Ravichandran, 2016). Thus, a well-established method for determining deficient efferocytosis is the Terminal deoxynucleotidyl transferase dUTP Nick-End Labeling (TUNEL) assay which labels secondary apoptotic cells. As expected, analysis of vehicle-treated tumors predominantly revealed that the majority of regions contained only 1 or 2 DAPI+ TUNEL+ (i.e., uncleared) apoptotic cells (**Figure 7E**, see far-left panel for representative image). Furthermore, regions of vehicle-treated tumors featuring higher numbers of DAPI+ TUNEL+ cells were entirely contained in small 'core-like' structures (**Figure 7E**, see center-left panel for representative image), suggesting that TAMs were still capable of containing potentially dangerous uncleared apoptotic cells similar to the anti-inflammatory macrophage behavior in granulomas (Locke et al., 2019; Wilson et al., 2019). On the other hand, tumors treated with 6-AN exhibited significantly more DAPI+ TUNEL+ cells, ranging from ~10 to ~300 uncleared apoptotic cells per region (**Figure 7E** see center- and far-right panels for representative image).

Furthermore, regions of 6AN-treated tumors featuring high numbers of DAPI+ TUNEL+ cells were highly disorganized with uncleared apoptotic cells pervading throughout the tumor parenchyma (**Figure 7E**, see far-right panel for representative image), suggesting that not only were TAMs less able to clear apoptotic cells, but also less capable of containing uncleared apoptotic cells into granulomatous structures. Thus, our data suggest that perturbation of PPP metabolism disrupts apoptotic cell clearance *in vivo*.

Discussion

Professional phagocytes, such as macrophages, reside in tissues throughout the body in limited nutrient environments often for long periods of time (Blériot et al., 2020; Guilliams et al., 2020). This is especially true for oxygen, which ranges between physoxia (38 mmHg, or ~5%) and physiological hypoxia (15 mmHg, or ~2%), with some tissues even lower (Carreau et al., 2011). Despite the relative dearth of oxygen, phagocytes remain responsible for removing millions of apoptotic cells daily (Norris et al., 2019), a process that is metabolically demanding and potentially perilous (Trzeciak et al., 2021). How phagocytes adapt to continuous inhabitance in low oxygen environments and how such adaptations inform clearance of apoptotic cells ('efferocytosis') remains unexplored. Here, we made the striking observation that macrophages conditioned in chronic hypoxia (~1% O_2) *in vitro* or *in vivo* become better phagocytes, both engulfing more apoptotic cells and degrading internalized apoptotic cells faster. As part of an adaptive response to prolonged hypoxia, macrophages induce two distinct states that support this enhanced efferocytosis. The first state, which we term 'primed', is characterized by concomitant changes in transcription and translation of programs, especially metabolic programs, in naïve macrophages that remain induced during efferocytosis. The second state, which we term 'poised', is characterized by transcription, but not translation, of phagocyte function programs in naïve macrophages that are subsequently translated during efferocytosis. We found that this primed state, in particular induction of a noncanonical pentose phosphate pathway loop that generates abundant NADPH, directly supports efficient efferocytosis (a core poised state program). Based on our findings, we propose that phagocytes that reside in physiological hypoxic environments, such as highly phagocytic macrophages in the bone marrow or spleen (Norris et al., 2019; Sender and Milo, 2021), adopt distinct states that both ensure their own fitness and their readiness to perform core homeostatic functions.

Previous analysis of phagocytosis in different oxygen levels has produced mixed findings. For instance, past studies have suggested that acute hypoxia enhances engulfment of opsonized targets (Acosta-Iborra et al., 2009), bacteria (Anand et al., 2007; Fritzenwanger et al., 2011), and apoptotic cells (Norris et al., 2019), whereas other studies have suggested that acute hypoxia has no effect on phagocytosis (Dehn et al., 2016; Fritzenwanger et al., 2011; Lin et al.,

2018) or decreases clearance of apoptotic cells (Marsch et al., 2014), and that macrophages in hypoxic regions may produce less of the anti-inflammatory mediatory IL-10 which is produced during efferocytosis (Zhang et al., 2019). Much of the contradiction might relate to variations in how hypoxia was induced/maintain or for how long cells were cultured in hypoxia, typically ranging from 3h to 24h. Indeed, significant cellular changes can occur, including degradation of HIF proteins and HIF-dependent transcriptional programs, as quickly as 24h after introduction to hypoxia (Ginouvès et al., 2008; Jain et al., 2020). Although we observed a modest increase in population-level efferocytosis in macrophages exposed to acute hypoxia, these cells did not exhibit enhanced lysosomal degradation. Instead, the most dramatic differences in both uptake and degradation of apoptotic cells were observed in macrophages conditioned in chronic hypoxia. Given our observation of concomitant loss of both HIF1α and HIF2α in chronic hypoxia-conditioned macrophages, we speculate that prolonged exposure to hypoxia induces distinct HIF-uncoupled programs that support efficient efferocytosis. This hypothesis is consistent with recent work demonstrating that macrophage efferocytosis occurs independent of HIF proteins, irrespective of whether cells are cultured in standard oxygen or acute hypoxia (Lin et al., 2018). It will be interesting to interrogate HIF-uncoupled efferocytosis programs further, especially considering phagocytes residing in physiological hypoxic tissues are often responsible for clearing biological material beyond conventional apoptotic cells (Trzeciak et al., 2021; Zago et al., 2021).

There is increased interest in how cells adapt metabolically to chronic hypoxia (CITE). For instance, Mootha and colleagues found that transformed cells (e.g., K562 cells) predominantly depend on lipid synthesis- and peroxisome biology-associated genes but not mitochondrial or Fe-S biosynthesis genes for survival in chronic hypoxia (Jain et al., 2020). In the present study, we observed downregulation of transcripts and proteins associated with mitochondrial and lipid metabolism as well as alterations in mitochondrial structure, oxidative state, and membrane potential, similar to changes observed in chronic hypoxia-conditioned THP1 monocyte-derived macrophages (Fuhrmann et al., 2013). Unique in the current study, we observed that chronic hypoxia-conditioned macrophages upregulate transcripts and proteins involved in glucose metabolism/gluconeogenesis as well as shunted glucose into a pentose

phosphate pathway (PPP)/gluconeogenesis loop, supporting the hypothesis that cells adapt to chronic hypoxia by dramatically altering their subcellular biology to favor mitochondria-independent metabolic processes.

Despite the growing body of work detailing how cells undergo metabolic adaptation to chronic hypoxia, understanding how such changes inform cellular function remains largely unexplored. Importantly, we move beyond a phenomenological understanding of cellular metabolic adaption to chronic hypoxia by mechanistically linking the changes in macrophage metabolism to enhanced apoptotic cell uptake and degradation. Unexpectedly, we found that macrophages under prolonged hypoxia limit glucose flux to most major pathways including anaerobic glycolysis and the TCA cycle. Instead, macrophages shunt glucose into a noncanonical PPP loop involving repeated cycling of PPP intermediates back to G6P via a process resembling gluconeogenesis. Importantly, we found that this PPP loop is necessary for generation of NADPH in naïve macrophages and appears to provide the NADPH necessary for appropriate phagolysosomal maturation and apoptotic cell degradation.

Previous studies of neutrophils and LPS-stimulated macrophages, both of which are thought to exist in an inflammatory state, have been shown to rely on PPP for function under standard oxygen (Baardman et al., 2018; Gonçalves et al., 2020; O'Neill et al., 2016). Although this raises the question of whether macrophages conditioned in chronic hypoxia are also inflammatory, several pieces of evidence counter this notion. First, it was previously shown that inflammatory macrophages, such as those elicited by LPS, have decreased efferocytosis potential compared to naïve macrophages (Feng et al., 2011; McPhillips et al., 2007; Michlewska et al., 2009; Thorp et al., 2011) whereas we observe increased efferocytosis potential in chronic hypoxia-conditioned macrophages. Second, the transcriptional and translational programs of chronic hypoxia-conditioned macrophages are similar to those observed in canonical pro-resolving macrophages, including expression of wound healing and anti-inflammatory programs highlighted by robust induction of Arginase 1 (ARG1). Finally, inflammatory macrophages and neutrophils exhibit increased glucose uptake, increased aerobic glycolysis and glucose-derived pyruvate generation, and increased TCA cycle activity (Cameron et al., 2019; Di Gioia et al., 2020; Liu et al., 2016), whereas chronic hypoxia-conditioned

macrophages display none of these changes. Although it remains possible that chronic hypoxia-conditioned macrophages exhibit some features of an inflammatory response, our findings suggest that the transcriptional/translational programs and metabolic pathways induced under prolonged hypoxia are distinct from those observed in canonical pro-inflammatory phagocytes.

A series of important questions that arise from our work relate to our observation that chronic hypoxia seems to induce both 'primed' and 'poised' states in macrophages. For instance, what macrophage functions, beyond efferocytosis, are 'poised' under chronic hypoxia? Efferocytosis is generally a core macrophage function shared across tissue-resident macrophage populations, but are there functions that are informed by a combination of oxygen availability and tissue-specific factors (e.g., presence of heme)? How do changes in oxygen availability during development inform efferocytosis potential? Finally, how are these poised programs regulated, for example, are they maintained by ribosomal stalling or increased chromatin accessibility/transcription? Although beyond the scope of the work presented here, answers to these questions could provide important clues on how macrophage function in specific environments maintain tissue homeostasis, or as preliminary data presented here suggest, support cancer progression.

STAR Methods

Contact for Reagent and Resource Sharing

For further information and requests for resources and reagents should be directed to the Lead Contact, Justin S. A. Perry (perryj@mskcc.org).

Standard Oxygen and Hypoxia Conditioning

To model standard oxygen, acute hypoxia, and chronic hypoxia environments, we optimized protocols using the BioSpherix Xvivo X3 system, which allows us to dynamically regulate CO_2 and O_2 (down to 0.1%) in four different chambers without exposing cells to atmosphere. Primary macrophage progenitors immortalized with a modified estrogen receptor-Hoxb8 fusion (ER-Hoxb8) were generated as previously reported (Wang et al., 2006) from C57BL/6J mice. Progenitors were maintained in RPMI 1640 containing 5% heat-inactivated fetal

bovine serum, 5% P885L (GM-CSF producing)-conditioned media, and 0.5μM β-estradiol (Sigma) in standard oxygen (~21% O_2). To differentiate into primary macrophages, progenitors were first washed three times with cold PBS to remove β-estradiol. Progenitors were then cultured in a-MEM containing 5% heat-inactivated fetal bovine serum, 1% Penicillin-Streptomycin-Glutamine (100X), and 10% L929 (M-CSF producing)-conditioned media. On day 6 of differentiation, mature macrophages were replated in non-TC treated plates and cultured in either standard oxygen or hypoxia (1% O_2) for 7 days prior to use in efferocytosis assays. For some experiments, progenitors were instead cultured in standard oxygen or hypoxia for 7 days prior to differentiation and use in efferocytosis assays. In all cases, media was replenished every other day and cells were incubated @37°C.

Induction of Apoptosis

For thymocyte engulfment, thymi from 6-week-old mice were harvested and crushed between frosted slides to release thymocytes. Cells were then treated with dexamethasone (50μM) for 4 hours prior to downstream use. Jurkat T lymphoma, MDA-MB-231, BrM2, and E0771 cells, were induced to undergo apoptosis by treatment with 150mJ cm^{-2} (Jurkat cells) or 650mJ cm^{-2} ultraviolet C irradiation (Stratalinker) at ~$5x10^6$ cell density per 10cm non-TC treated dish. Then, cells were incubated for 4h, 8h, 16h, or 24h before downstream use. Apoptosis was confirmed via Annexin V/7-AAD staining to be greater than 70% Annexin V+ single-positive (Figure S1A).

In Vitro Efferocytosis Assays

Apoptotic cells were stained with either 1μM CypHer5E (Cytiva) or 50μM TAMRA-SE (ThermoFisher) in serum-free HBSS for 45min. Then, cells were washed by incubating in serum-containing assay media for an additional 25min. Apoptotic cells were co-cultured with macrophages at a 1:1 phagocyte to target ratio. All efferocytosis assays included four technical replicates for each condition with at least three biological replicates. For all pharmacological studies, phagocytes were pre-incubated with the compounds listed below or vehicle (DMSO) for 16h or 6d prior to addition of apoptotic cells. Macrophages were treated with the following:

6-AN (MedChemExpress, 100μM), G6PDi-1 (Cayman Chemical, 50μM), or FBP1i (Cayman Chemical, 25μM). Macrophages were examined via microscopy to ensure no gross morphological changes or cell death had occurred due to drug treatment. Macrophages and apoptotic cells were co-cultured for 1h. Apoptotic cells were subsequently removed via three washes with cold assay media and phagocytes were harvested using a cell scraper (Biotium) and assessed by flow cytometry. For continual efferocytosis, the first round of apoptotic cells was labeled with CFSE (ThermoFisher) and co-cultured with macrophages at a 1:1 ratio for 1h. Then, apoptotic cells were washed away using cold assay media. Macrophages were subsequently rested for 1.5h prior to co-culture with a second round of apoptotic cells that were labeled with CypHer5E. Continual efferocytosis was assessed by FACS as CFSE+ (1st corpse uptake) and CFSE+ CypHer5E+ (2nd corpse uptake) macrophages. FACS analysis was performed using an Attune NxT Flow Cytometer (ThermoFisher) and analyzed using FlowJo 10.7.1.

Time-lapse Confocal Microscopy

Equipment. Experiments to evaluate per cell uptake and degradation were performed on a Zeiss Axio Observer.Z1 7 inverted fluorescence microscope equipped with a Zeiss 20x Plan-Apo (0.8 NA) objective, a 6-channel, 7-laser LSM 980 (405nm, 445nm, 488nm, 514nm, 561nm, 594nm, 639nm), and a Airyscan 2 multiplex detector. The imaging stage is fully encased in a black-out environmental chamber and the Z PIEZO stage is fully encapsulated with a heating/gas-controlled insert, together allowing us to control the temperature, humidity, CO_2, and O_2. Time-lapse experiments were acquired using Zen Blue software (Zeiss).

Experiment. Prior to imaging, cells were allowed to acclimate for at least 10min. After selection of scenes (see below), apoptotic cells were added to phagocyte-containing chamber slides and scenes were rapidly focused prior to the beginning of data collection. For each condition/experiment, at least 8 regions ('scenes') were selected and imaged. Scenes were selected if they featured at least 10 cells per region, and when experimental manipulations were performed (e.g., 6-AN treatment), regions were selected that featured similar cell numbers between vehicle and treatment conditions. Scenes were imaged every 4min for a minimum of 8h per experiment, which generally equates to ~0.5μs per pixel or 5s per scene.

Time-lapse experiments were performed in Multiplex CO-8Y mode which allows for gentle confocal-resolution imaging at a high frame rate. Specifically, we set the pinhole to 2.42 Airy units (57μm) with the image scaling (per pixel) set at 0.414μm x 0.414μm with 2x averaging. Focusing was ensured using the Definite Focus 2 module with a two-part strategy that was first based on the initial focus of individual scenes and then subsequently updated after each round of images. Analysis, including generation of scale bars, was performed using Zen Blue or Fiji.

Ex vivo Efferocytosis

To perform ex vivo efferocytosis, tissues were isolated from 7-week-old female C57BL/6 mice. To isolate bone marrow-resident macrophages (BMMs), bone marrow was flushed from bones using a 25G needle with α-MEM media containing FBS in a hypoxia chamber set to 1% oxygen. Red blood cells were lysed, and remaining bone marrow cells were plated in a non-TC-treated 6-well plate in BMDM media and cultured overnight in either hypoxia (1%) or standard (21%) oxygen. Floating cells were removed and fresh BMDM media was added. BMMs were then co-cultured with CypHer5E-labeled apoptotic MDA-MD-231 cells at a 1:1 ratio for 1h. Macrophages were isolated, stained with CD11b and F4/80, and analyzed via flow cytometry. To isolate splenic macrophages, spleens were minced into small pieces in a hypoxia chamber set to 1% oxygen and digested for 20min at 37C. Cell suspensions were strained using a 70μm cell strainer. Red blood cells were lysed, and remaining splenic cells were plated and treated identical to bone marrow-resident macrophages as described above.

RNA Sequencing

For bulk RNA sequencing, $4.5x10^5$ macrophages were conditioned for 7d in standard O_2 (~21%) and either immediately collected or pulsed with 3h of 1% O_2 (acute) and then collected. In parallel, $4.5x10^5$ macrophages were conditioned for 7d in 1% O_2 (chronic) then collected. Collected samples were subsequently collected, washed with cold PBS, and lysed on ice with beta-mercaptoethanol-containing lysis buffer (Buffer RA, Machery-Nagel) for downstream RNA isolation. Total RNA was isolated using the NucleoSpin RNA isolation kit with on-column rDNase digestion (Machery-Nagel) and mRNA libraries were generated by polyA capture and reverse

transcription of cDNA. Libraries were then sequenced at 150bp (paired-end) reads with ~20 million reads per sample using an Illumina NovaSeq 6000 sequencer.

Proteomics

For ^{13}C SILAC labeling, target cells were grown in lysine- and arginine-deficient DMEM with 10% dialyzed FBS, 1% PSQ, and 2mM L-glutamine, supplemented with 'heavy' $^{13}C_6$-lysine and 'light' $^{12}C_6$-arginine (100mg/L; Cambridge Isotope Laboratories). After 8–10 passages, incorporation of $^{13}C_6$-lysine-labeled amino acids into proteins was verified via LC-MS/MS to be >99%. Heavy isotope-labeled target cells were expanded in $^{13}C_6$-lysine media and induced to undergo apoptosis. Macrophages were first conditioned in standard oxygen or hypoxia (see above), and then cultured with or without apoptotic cells for 1h. Apoptotic cells were subsequently removed using two cold assay media washes and two cold PBS washes. Macrophages were then removed using a cell scraper, pelleted to remove any residual liquid, and immediately snap frozen on dry ice.

Sample Preparation. Cell pellets were lysed with 200-300 µL buffer containing 8M urea and 200mM EPPS (pH at 8.5) with protease inhibitor (Roche) and phosphatase inhibitor cocktails 2 and 3 (Sigma). Lysates were aspirated 2x on ice, followed by water sonication for 2min @4°C. Benzonase (Millipore) was added to a concentration of 50u/mL and incubated on ice for 15min. Samples were centrifuged at 14,000g for 10 min (@4°C) and the supernatant was subsequently extracted. The Pierce bicinchoninic acid (BCA) protein concentration assay was used to determine protein concentration. Protein disulfide bonds were reduced with 5mM tris (2-carboxyethyl) phosphine (@RT, 30min), then alkylated with 10mM iodoacetamide (@RT, 30min, in the dark). The reaction was quenched with 10mM dithiothreitol (@RT, 15min). Equivalent volumes of lysate aliquots were taken for each sample (100–200µg in each sample) and diluted to approximately 100µL with lysis buffer. Samples were subjected to chloroform/methanol precipitation as previously described (CITE 1). Pellets were reconstituted in 100µL of 200mM EPPS buffer and digested with Lys-C (1:100 enzyme-to-protein ratio) and incubated @37°C for 4h. Trypsin was then added (1:100 enzyme-to-protein ratio) and digested @37°C overnight. Anhydrous acetonitrile was then added to make a final volume of 30% ACN.

TMT Labeling. Samples were TMT-labeled as described (CITE 1). Briefly, samples were TMT-tagged by adding 10µL (28µg/µL) of TMTPro reagent for each sample and incubated for 1h @RT. A ratio check was performed by taking a 2µL aliquot from each sample and desalted by the StageTip method (CITE 2) to confirm labeling efficiency. TMT-tags were then quenched with hydroxylamine to a final concentration of 0.3% for 15min @RT. Samples were pooled in their entirety, then dried via vacuum-centrifugation. Dried samples were reconstituted in 1mL of 3% ACN/1% TFA, desalted using a 100mg tC18 SepPak (Waters), and lyophilized overnight. Lyophilized peptides were dried using vacuum-centrifugation and reconstituted in 1mL of 2% ACN/25mM ABC. Peptides were fractionated into 48 fractions. Next, an Ultimate 3000 HPLC (Dionex) coupled to an Ultimate 3000 Fraction Collector using a Waters XBridge BEH130 C18 column (3.5µm x 4.6mm x 250mm) was operated at 1mL/min. The Buffers A, B, and C used below consisted of 100% water, 100% ACN, and 25mM ABC, respectively. The fractionation gradient operated as follows: 1% B to 5% B in 1min, 5% B to 35% B in 61min, 35% B to 60% B in 5min, 60% B to 70% B in 3min, 70% B to 1% B in 10min, with 10% C the entire gradient to maintain pH. The 48 fractions were then concatenated to 12 fractions (i.e., fractions 1, 13, 25, 37 were pooled, followed by fractions 2, 14, 26, 38, etc.) so that every 12th fraction was used to pool. Pooled fractions were vacuum-centrifuged then reconstituted in 1% ACN/0.1% FA for LC-MS/MS.

LC-MS/MS. Total fractions were analyzed by LC-MS/MS using a NanoAcquity (Waters) with a 50cm EASY-Spray Column (PepMap RSLC, C18, 2µm, 100Å, 75µm I.D.) heated to 60°C coupled to a Orbitrap Eclipse Tribrid Mass Spectrometer (Thermo Fisher Scientific). Peptides were separated by direct inject at a flow rate of 300nL/min using a gradient of 5 to 30% acetonitrile (0.1% FA) in water (0.1% FA) over 3h then to 50% ACN in 30min and analyzed by SPS-MS3. MS1 scans were acquired over a range of m/z 375-1500, 120K resolution, AGC target (4.0e5), and maximum IT of 50ms. MS2 scans were acquired on MS1 scans of charge 2-7 using an isolation of 0.7m/z, collision induced dissociation with activation of 32%, turbo scan and max IT of 50ms. MS3 scans were acquired using specific precursor selection (SPS) of 10 isolation notches, m/z range 100-1000, 50K resolution, AGC target (1.0e5), HCD activation of 45%, and max IT of 150ms. The dynamic exclusion was set at 60s.

TMT Data Analysis. Raw data files were processed using Proteome Discoverer (PD) version 2.4.1.15 (Thermo Scientific). For each of the TMT experiments, raw files from all fractions were merged and searched with the SEQUEST HT search engine with a UniProt protein database downloaded on 2019/01/09 (176,945 entries). The precursor and fragment mass tolerances were 10ppm and 0.6Da respectively. A maximum of two trypsin missed cleavages were permitted. Searches used a reversed sequence decoy strategy to control peptide false discovery rate (FDR) and 1% FDR was set as threshold for identification.

Analysis of Nutrient Consumption and Secretion via YSI

Macrophages ($2.5x10^6$) were cultured in either standard oxygen or hypoxia (1% O_2) and conditioned for a total of 7 days. Media was changed at day 1, day 3, and day 5 prior to a 24h period of conditioning. At the end of the 24h period (denoted as day 2-3, day 4-5, and day 6-7 periods), media was collected, spun down to remove cell debris, and immediately snap frozen for downstream analysis via a 2950D Biochemistry Analyzer (YSI Life Sciences) to determine glucose and lactate concentrations. Absolute rates of consumption (glucose) or secretion (lactate) were calculated first by subtracting the concentration observed in control (cell-free) media incubated in parallel, then normalized to cell number and volume of media. These experiments were performed independently at least two times.

Untargeted Metabolomics

Macrophages ($2.5x10^6$) were conditioned in standard oxygen or hypoxia for 7d. To protect from experimental artifact, all samples were collected in the same oxygen environment that they were conditioned in. Plates containing cells were placed on ice and washed with cold PBS three times, then moved to dry ice and ice cold 80% methanol was added. Cells were subsequently scraped and transferred to a cold centrifuge tube on dry ice. The cell-methanol slurries were then vortexed for 1min, allowed to rest on dry ice for 5min, then vortexed an additional 1min to create cell lysates. Lysates were centrifuged for 20min at 14,000g in a refrigerated centrifuge set to 4°C to remove debris. Supernatants were transferred to clean tubes and lyophilized in the absence of heat and dissolved in water. Targeted LC/MS analyses

were performed on a Q Exactive Orbitrap mass spectrometer (Thermo Scientific) coupled to a Vanquish UPLC system (Thermo Scientific). The Q Exactive operated in polarity-switching mode. A Sequant ZIC-HILIC column (2.1mm i.d. × 150mm, Merck) was used for separation of metabolites. Flow rate was set at 150µL/min. Buffers consisted of 100% acetonitrile for mobile B, and 0.1% NH4OH/20mM CH3COONH4 in water for mobile A. Gradient ran from 85% to 30% B in 20min followed by a wash with 30% B and re-equilibration at 85% B. MS data were processed using Compound Discoverer (Thermo Scientific). An in-house metabolite library as well as Chemspider were searched for metabolite identification. Three levels of metabolite identification were reported: 1) identified compounds: definitive identification based on the mass (within 5ppm) and retention time of authentic chemical standards; 2) putatively annotated compounds by searching ChemSpider (mass tolerance 5ppm); 3) compounds with predicted chemical composition based on mass. Relative metabolite quantitation was performed based on peak area for each metabolite. Hierarchical clustering analysis and principal component analysis (PCA) were performed by Compound Discoverer (Thermo Scientific).

^{13}C-Metabolic Flux Analysis

Experiments were performed similar to those outlined in Untargeted Metabolomics with the following modification. On day 5, glucose-deficient RPMI containing 1 g/L [1,2-^{13}C]-glucose or [U-^{13}C]-glucose (both from Cambridge Isotope Laboratories), 10% L929-conditioned media, 1% PSQ, and 10% FBS was conditioned in either standard oxygen or hypoxia for 16-24h. On day 6, conditioned macrophages were washed with PBS twice and then cultured with heavy isotope-containing media for 16h. Metabolites were extracted using the same protocol detailed in Untargeted Metabolomics. LC/MS analyses were performed on a Q Exactive Orbitrap mass spectrometer (Thermo Scientific) coupled to a Vanquish UPLC system (Thermo Scientific). The Q Exactive operated in polarity-switching mode. A Sequant ZIC-HILIC column (2.1mm i.d. × 150mm, Merck) was used for separation of metabolites. Flow rate was set at 150µL/min. Buffers consisted of 100% acetonitrile for mobile B, and 0.1% NH4OH/20mM CH3COONH4 in water for mobile A. Gradient ran from 85% to 30% B in 20min followed by a wash with 30% B

and re-equilibration at 85% B. Data analysis was done using El-MAVEN (v0.12.0). Metabolites and their ^{13}C isotopologues were identified on the basis of exact mass within 5ppm and standard retention times. Relative metabolite quantitation was performed based on peak area for each metabolite.

Analysis of Mitochondrial Properties

For analysis of mitochondrial superoxide levels, conditioned macrophages were labeled with the live cell-permeant fluorogenic probe MitoSOX Red (ThermoFisher). MitoSOX Red is targeted to the mitochondria and is oxidized by superoxide but not reactive oxygen or nitrogen species, inducing an increase in fluorescence which we quantified using flow cytometry. To estimate mitochondrial shape and content, conditioned macrophages were labeled with both MitoTracker Green (MTG) and MitoTracker Deep Red (MTDR, both ThermoFisher). MTG localizes to mitochondria independent of mitochondrial membrane potential whereas MTDR labeling of mitochondria is dependent on mitochondrial membrane potential. Combined, the two fluorogenic probes were used to estimate shape (via confocal microscopy) and quantity (via flow cytometry).

NADP+/NADPH and GSH/GSSG Measurement

Either $4x10^6$ or $2.5x10^4$ macrophages were seeded for conditioning and subsequent NADP+/NADPH or GSH/GSSG measurement, respectively. In some experiments, macrophages were treated with 6-AN (100nM) or vehicle (DMSO) beginning one day after replating. On day 7, cells were collected, processed, and the ratio of NADP+/NADPH or GSH/GSSG was measure using the NADP/NADPH Quantitation Colorimetric Kit (BioVision) or the GSH/GSSG-Glo Assay (Promega), respectively, following the manufacturer's protocol.

Measurement of Redox State and Lysosomal Acidity

Lipid peroxidation and cellular ROS was determined by labeling of phagocytes using the reagent BODIPY 581/591 C11 and CellROX Deep Red (both ThermoFisher), respectively, followed by flow cytometric analysis. Lysosomal acidity was determined by labeling of

phagocytes using the reagent Lysosensor Green DND-189. Labeling was performed according to manufacturer instructions. For analysis of redox state or lysosomal acidity in efferocytotic cells, phagocytes were first gated on CypHer5E+.

Orthotopic Breast Cancer Model

Female, 7-week-old C57BL/6J mice were obtained from Jackson Laboratories and allowed to acclimate for one week. Orthotopic mammary fat pad implantation of breast cancer cells was performed as follows: mice were injected with $5x10^5$ E0771 resuspended in a 50/50 mix of PBS and Matrigel (40μl of each) into the mammary fat pad. Sterile tweezers were used to lift the right forth nipple and a 26G syringe needle was used to implant cell suspensions directly into the mammary fat pad. Mice were randomly assigned to vehicle or 6-Aminonicotinamide (6-AN) treatment groups. Treatment with vehicle or 6-AN (MedChemExpress, 3mg/kg in 10% DMSO, 40% PEG300, 5% Tween-80, and 45% saline) began five days after inoculation and continued for five consecutive days, then switched to treatment every other day. Body weights and tumor size [length (L) and width (W)] were measured using calipers, and tumor volume (vol) was calculated as [$vol = (L \times W^2)/2$]. Tumors were collected for downstream immune cell characterization. All animal procedures were performed according to the protocols provided by the Institutional Animal Care and Use Committee (IACUC) of Memorial Sloan Kettering Cancer Center.

Tumor-Associated Immune Cell Analysis

For flow cytometric analysis of tumor-associated immune cells, orthotopically-implanted E0771 tumors were resected, washed with PBS once to remove residual blood, and then mechanically dissociated with surgical scissors. To generate single cell suspensions, tumor tissues were digested for 30min at 37°C in HBSS containing type IV collagenase (0.5mg/ml), DNase I (40U/ml), hyaluronidase (0.2mg/ml), and $CaCl_2$ (5mM). Cell suspensions were strained using a 70μm cell strainer and red blood cells were lysed using ammonium chloride potassium (ACK) lysis buffer. Single cell suspensions were first incubated with a Fc receptor (CD16/CD32)-blocking antibody (clone 2.4G2; BioXCell). Then, cells were labeled with antibodies to identify

indicated immune cell subsets. Intracellular staining of Foxp3 and Arginase-1 was performed according to the manufacturer's instructions. LIVE/DEAD Fixable Aqua Dead Cell Stain (ThermoFisher) was used to exclude dead cells from analysis. Samples were analyzed using an Attune NxT flow cytometer.

Statistics and Reproducibility

Statistical analyses were executed using GraphPad Prism 7, SPSS v.22, and R v.4.0.5. We determined statistical significance, depending on the structure of the data, via unpaired two-tailed Student's t-test, nonparametric Mann–Whitney U-test, one-way or two-way ANOVA, or Fisher's exact test. R v.4.0.5 was used for graphical and statistical analyses and the R package DESeq2 was used for differential gene expression analysis of transcriptomic and proteomic analyses. All genes were curated according to a previously described approach (Morioka et al., 2018). Complementary analyses of biological pathways were performed by comparing significantly differentially expressed genes or proteins and cross-referencing them with the Molecular Signatures Database (MSigDB). Gephi (v.0.9.1 https://gephi.org/) was used to perform standard network clustering analyses. The "Link Communities" algorithm for biological network analysis was used to calculate edges and nodes (Ahn et al., 2010). The Yifan Hu layout algorithm was used to determine network structure. All biologically independent samples were included and used for statistical and graphical analyses. No data was excluded from this manuscript. Sample sizes were not predetermined using statistical methods. The code used in this manuscript is available upon reasonable request.

Acknowledgements

We thank members of the Perry laboratory and co-authors for discussions related to this manuscript. We thank Justin Cross and the Donald B. and Catherine C. Marron Cancer Metabolism Center at MSKCC for help with YSI experiments. This work was supported by grants to J.S.A.P. from the NIH (NCI 5R00CA237728; NIGMS 1DP2GM146337), a Parker Institute for Cancer Immunotherapy Career Development Award, a V Foundation Scholars Award, a MSKCC Functional Genomics Institute pilot award, a grant to K.R.K. from the NIH (NCI 1R01CA248364),

and MSKCC Cancer Center Support Grant P30CA008748. Some panels in figures were created using BioRender.

Competing Financial Interests

The authors declare no competing financial interests.

References

Acosta-Iborra, B., Elorza, A., Olazabal, I.M., Martín-Cofreces, N.B., Martin-Puig, S., Miró, M., Calzada, M.J., Aragonés, J., Sánchez-Madrid, F., and Landázuri, M.O. (2009). Macrophage oxygen sensing modulates antigen presentation and phagocytic functions involving IFN-gamma production through the HIF-1 alpha transcription factor. Journal of immunology (Baltimore, Md : 1950) *182*, 3155-3164.

Ahn, Y.-Y., Bagrow, J.P., and Lehmann, S. (2010). Link communities reveal multiscale complexity in networks. Nature *466*, 761-764.

Alexandrou, S., George, S.M., Ormandy, C.J., Lim, E., Oakes, S.R., and Caldon, C.E. (2019). The Proliferative and Apoptotic Landscape of Basal-like Breast Cancer. Int J Mol Sci *20*, 667.

Amit, I., Winter, D.R., and Jung, S. (2016). The role of the local environment and epigenetics in shaping macrophage identity and their effect on tissue homeostasis. Nature Immunology *17*, 18-25.

Anand, R.J., Gribar, S.C., Li, J., Kohler, J.W., Branca, M.F., Dubowski, T., Sodhi, C.P., and Hackam, D.J. (2007). Hypoxia causes an increase in phagocytosis by macrophages in a HIF-1α-dependent manner. *82*, 1257-1265.

Artyomov, M.N., and Van den Bossche, J. (2020). Immunometabolism in the Single-Cell Era. Cell Metabolism *32*, 710-725.

Baardman, J., Verberk, S.G.S., Prange, K.H.M., van Weeghel, M., van der Velden, S., Ryan, D.G., Wüst, R.C.I., Neele, A.E., Speijer, D., Denis, S.W*., et al.* (2018). A Defective Pentose Phosphate Pathway Reduces Inflammatory Macrophage Responses during Hypercholesterolemia. Cell Reports *25*, 2044-2052.e2045.

Bagaitkar, J., Huang, J., Zeng, M.Y., Pech, N.K., Monlish, D.A., Perez-Zapata, L.J., Miralda, I., Schuettpelz, L.G., and Dinauer, M.C. (2018). NADPH oxidase activation regulates apoptotic neutrophil clearance by murine macrophages. Blood *131*, 2367-2378.

Bianchini, G., Balko, J.M., Mayer, I.A., Sanders, M.E., and Gianni, L. (2016). Triple-negative breast cancer: challenges and opportunities of a heterogeneous disease. Nature Reviews Clinical Oncology *13*, 674.

Blériot, C., Chakarov, S., and Ginhoux, F. (2020). Determinants of Resident Tissue Macrophage Identity and Function. Immunity *52*, 957-970.

Boada-Romero, E., Martinez, J., Heckmann, B.L., and Green, D.R. (2020). The clearance of dead cells by efferocytosis. Nature Reviews Molecular Cell Biology *21*, 398-414.

Bosurgi, L., Cao, Y.G., Cabeza-Cabrerizo, M., Tucci, A., Hughes, L.D., Kong, Y., Weinstein, J.S., Licona-Limon, P., Schmid, E.T., Pelorosso, F*., et al.* (2017). Macrophage function in tissue repair and remodeling requires IL-4 or IL-13 with apoptotic cells. Science *356*, 1072-1076.

Breed, E.R., Watanabe, M., and Hogquist, K.A. (2019). Measuring Thymic Clonal Deletion at the Population Level. Journal of immunology (Baltimore, Md : 1950) *202*, 3226-3233.

Cameron, A.M., Castoldi, A., Sanin, D.E., Flachsmann, L.J., Field, C.S., Puleston, D.J., Kyle, R.L., Patterson, A.E., Hässler, F., Buescher, J.M*., et al.* (2019). Inflammatory macrophage dependence on NAD+ salvage is a consequence of reactive oxygen species–mediated DNA damage. Nature Immunology *20*, 420-432.

Carreau, A., El Hafny-Rahbi, B., Matejuk, A., Grillon, C., and Kieda, C. (2011). Why is the partial oxygen pressure of human tissues a crucial parameter? Small molecules and hypoxia. J Cell Mol Med *15*, 1239-1253.

Cheng, M.-L., Lin, J.-F., Huang, C.-Y., Li, G.-J., Shih, L.-M., Chiu, D.T.-Y., and Ho, H.-Y. (2019). Sedoheptulose-1,7-bisphospate Accumulation and Metabolic Anomalies in Hepatoma Cells Exposed to Oxidative Stress. Oxidative Medicine and Cellular Longevity *2019*, 5913635.

Cook, R.S., Jacobsen, K.M., Wofford, A.M., DeRyckere, D., Stanford, J., Prieto, A.L., Redente, E., Sandahl, M., Hunter, D.M., Strunk, K.E*., et al.* (2013). MerTK inhibition in tumor leukocytes decreases tumor growth and metastasis. The Journal of Clinical Investigation *123*, 3231-3242.

Dehn, S., DeBerge, M., Yeap, X.-Y., Yvan-Charvet, L., Fang, D., Eltzschig, H.K., Miller, S.D., and Thorp, E.B. (2016). HIF-2α in Resting Macrophages Tempers Mitochondrial Reactive Oxygen Species To Selectively Repress MARCO-Dependent Phagocytosis. *197*, 3639-3649.
Denko, N.C. (2008). Hypoxia, HIF1 and glucose metabolism in the solid tumour. Nature Reviews Cancer *8*, 705-713.
Di Gioia, M., Spreafico, R., Springstead, J.R., Mendelson, M.M., Joehanes, R., Levy, D., and Zanoni, I. (2020). Endogenous oxidized phospholipids reprogram cellular metabolism and boost hyperinflammation. Nat Immunol *21*, 42-53.
Doran, A.C., Yurdagul, A., and Tabas, I. (2020). Efferocytosis in health and disease. Nature Reviews Immunology *20*, 254-267.
Egelston, C.A., Avalos, C., Tu, T.Y., Rosario, A., Wang, R., Solomon, S., Srinivasan, G., Nelson, M.S., Huang, Y., Lim, M.H.*, et al.* (2019). Resident memory CD8+ T cells within cancer islands mediate survival in breast cancer patients. JCI Insight *4*.
Elliott, Michael R., and Ravichandran, Kodi S. (2016). The Dynamics of Apoptotic Cell Clearance. Developmental Cell *38*, 147-160.
Feng, X., Deng, T., Zhang, Y., Su, S., Wei, C., and Han, D. (2011). Lipopolysaccharide inhibits macrophage phagocytosis of apoptotic neutrophils by regulating the production of tumour necrosis factor α and growth arrest-specific gene 6. Immunology *132*, 287-295.
Fritzenwanger, M., Jung, C., Goebel, B., Lauten, A., and Figulla, H.R. (2011). Impact of short-term systemic hypoxia on phagocytosis, cytokine production, and transcription factor activation in peripheral blood cells. Mediators Inflamm *2011*, 429501-429501.
Fuhrmann, D.C., Wittig, I., Heide, H., Dehne, N., and Brüne, B. (2013). Chronic hypoxia alters mitochondrial composition in human macrophages. Biochimica et biophysica acta *1834*, 2750-2760.
Ginouvès, A., Ilc, K., Macías, N., Pouysségur, J., and Berra, E. (2008). PHDs overactivation during chronic hypoxia "desensitizes" HIFα and protects cells from necrosis. *105*, 4745-4750.
Gonçalves, S.M., Duarte-Oliveira, C., Campos, C.F., Aimanianda, V., ter Horst, R., Leite, L., Mercier, T., Pereira, P., Fernández-García, M., Antunes, D.*, et al.* (2020). Phagosomal removal of fungal melanin reprograms macrophage metabolism to promote antifungal immunity. Nature Communications *11*, 2282.
Guilliams, M., and Svedberg, F.R. (2021). Does tissue imprinting restrict macrophage plasticity? Nature Immunology *22*, 118-127.
Guilliams, M., Thierry, G.R., Bonnardel, J., and Bajenoff, M. (2020). Establishment and Maintenance of the Macrophage Niche. Immunity *52*, 434-451.
Henson, P.M. (2017). Cell Removal: Efferocytosis. Annual Review of Cell and Developmental Biology *33*, 127-144.
Hers, H.G., and Hue, L. (1983). Gluconeogenesis and related aspects of glycolysis. Annual review of biochemistry *52*, 617-653.
Hill, D.A., Lim, H.-W., Kim, Y.H., Ho, W.Y., Foong, Y.H., Nelson, V.L., Nguyen, H.C.B., Chegireddy, K., Kim, J., Habertheuer, A.*, et al.* (2018). Distinct macrophage populations direct inflammatory versus physiological changes in adipose tissue. *115*, E5096-E5105.
Huang, Y., Ma, C., Zhang, Q., Ye, J., Wang, F., Zhang, Y., Hunborg, P., Varvares, M.A., Hoft, D.F., Hsueh, E.C.*, et al.* (2015). CD4+ and CD8+ T cells have opposing roles in breast cancer progression and outcome. Oncotarget *6*, 17462-17478.
Jain, I.H., Calvo, S.E., Markhard, A.L., Skinner, O.S., To, T.-L., Ast, T., and Mootha, V.K. (2020). Genetic Screen for Cell Fitness in High or Low Oxygen Highlights Mitochondrial and Lipid Metabolism. Cell *181*, 716-727.e711.
Jang, C., Chen, L., and Rabinowitz, J.D. (2018). Metabolomics and Isotope Tracing. Cell *173*, 822-837.

Lee, P., Chandel, N.S., and Simon, M.C. (2020). Cellular adaptation to hypoxia through hypoxia inducible factors and beyond. Nature Reviews Molecular Cell Biology *21*, 268-283.
Lee, Y.-S., Kim, M.-H., Yi, H.-S., Kim, S.Y., Kim, H.-H., Kim, J.H., Yeon, J.E., Byun, K.S., Byun, J.-S., and Jeong, W.-I. (2018). CX3CR1 differentiates F4/80low monocytes into pro-inflammatory F4/80high macrophages in the liver. Scientific Reports *8*, 15076.
Lin, N., Shay, J.E.S., Xie, H., Lee, D.S.M., Skuli, N., Tang, Q., Zhou, Z., Azzam, A., Meng, H., Wang, H*., et al.* (2018). Myeloid Cell Hypoxia-Inducible Factors Promote Resolution of Inflammation in Experimental Colitis. Frontiers in Immunology *9*.
Liu, L., Lu, Y., Martinez, J., Bi, Y., Lian, G., Wang, T., Milasta, S., Wang, J., Yang, M., Liu, G*., et al.* (2016). Proinflammatory signal suppresses proliferation and shifts macrophage metabolism from Myc-dependent to HIF1α-dependent. *113*, 1564-1569.
Locke, L.W., Crouser, E.D., White, P., Julian, M.W., Caceres, E.G., Papp, A.C., Le, V.T., Sadee, W., and Schlesinger, L.S. (2019). IL-13-regulated Macrophage Polarization during Granuloma Formation in an In Vitro Human Sarcoidosis Model. Am J Respir Cell Mol Biol *60*, 84-95.
Longenecker, J.P., and Williams, J.F. (1980). Quantitative measurement of the L-type pentose phosphate cycle with [2-14C]glucose and [5-14C]glucose in isolated hepatocytes. The Biochemical journal *188*, 859-865.
Luo, B., Gan, W., Liu, Z., Shen, Z., Wang, J., Shi, R., Liu, Y., Liu, Y., Jiang, M., Zhang, Z*., et al.* (2016). Erythropoeitin Signaling in Macrophages Promotes Dying Cell Clearance and Immune Tolerance. Immunity *44*, 287-302.
Makowski, L., Chaib, M., and Rathmell, J.C. (2020). Immunometabolism: From basic mechanisms to translation. *295*, 5-14.
Mantegazza, A.R., Savina, A., Vermeulen, M., Pérez, L., Geffner, J., Hermine, O., Rosenzweig, S.D., Faure, F., and Amigorena, S. (2008). NADPH oxidase controls phagosomal pH and antigen cross-presentation in human dendritic cells. Blood *112*, 4712-4722.
Marsch, E., Theelen, T.L., Demandt, J.A., Jeurissen, M., van Gink, M., Verjans, R., Janssen, A., Cleutjens, J.P., Meex, S.J., Donners, M.M*., et al.* (2014). Reversal of hypoxia in murine atherosclerosis prevents necrotic core expansion by enhancing efferocytosis. Arteriosclerosis, thrombosis, and vascular biology *34*, 2545-2553.
McPhillips, K., Janssen, W.J., Ghosh, M., Byrne, A., Gardai, S., Remigio, L., Bratton, D.L., Kang, J.L., and Henson, P. (2007). TNF-alpha inhibits macrophage clearance of apoptotic cells via cytosolic phospholipase A2 and oxidant-dependent mechanisms. Journal of immunology (Baltimore, Md : 1950) *178*, 8117-8126.
Medrek, C., Pontén, F., Jirström, K., and Leandersson, K. (2012). The presence of tumor associated macrophages in tumor stroma as a prognostic marker for breast cancer patients. BMC Cancer *12*, 306.
Mehanna, J., Haddad, F.G., Eid, R., Lambertini, M., and Kourie, H.R. (2019). Triple-negative breast cancer: current perspective on the evolving therapeutic landscape. Int J Womens Health *11*, 431-437.
Michlewska, S., Dransfield, I., Megson, I.L., and Rossi, A.G. (2009). Macrophage phagocytosis of apoptotic neutrophils is critically regulated by the opposing actions of pro-inflammatory and anti-inflammatory agents: key role for TNF-alpha. FASEB journal : official publication of the Federation of American Societies for Experimental Biology *23*, 844-854.
Morioka, S., Maueröder, C., and Ravichandran, K.S. (2019). Living on the Edge: Efferocytosis at the Interface of Homeostasis and Pathology. Immunity *50*, 1149-1162.
Morioka, S., Perry, J.S.A., Raymond, M.H., Medina, C.B., Zhu, Y., Zhao, L., Serbulea, V., Onengut-Gumuscu, S., Leitinger, N., Kucenas, S*., et al.* (2018). Efferocytosis induces a novel SLC program to promote glucose uptake and lactate release. Nature *563*, 714-718.
Muri, J., and Kopf, M. (2020). Redox regulation of immunometabolism. Nature Reviews Immunology.

Norris, P.C., Libreros, S., and Serhan, C.N. (2019). Resolution metabolomes activated by hypoxic environment. *5*, eaax4895.
O'Neill, L.A.J., Kishton, R.J., and Rathmell, J. (2016). A guide to immunometabolism for immunologists. Nature Reviews Immunology *16*, 553-565.
Okabe, Y., and Medzhitov, R. (2016). Tissue biology perspective on macrophages. Nature Immunology *17*, 9-17.
Park, D., Han, C.Z., Elliott, M.R., Kinchen, J.M., Trampont, P.C., Das, S., Collins, S., Lysiak, J.J., Hoehn, K.L., and Ravichandran, K.S. (2011). Continued clearance of apoptotic cells critically depends on the phagocyte Ucp2 protein. Nature *477*, 220-224.
Penberthy, K.K., Lysiak, J.J., and Ravichandran, K.S. (2018). Rethinking Phagocytes: Clues from the Retina and Testes. Trends Cell Biol *28*, 317-327.
Perry, J.S.A., Morioka, S., Medina, C.B., Iker Etchegaray, J., Barron, B., Raymond, M.H., Lucas, C.D., Onengut-Gumuscu, S., Delpire, E., and Ravichandran, K.S. (2019). Interpreting an apoptotic corpse as anti-inflammatory involves a chloride sensing pathway. Nature Cell Biology *21*, 1532-1543.
Rothlin, C.V., Hille, T.D., and Ghosh, S. (2020). Determining the effector response to cell death. Nat Rev Immunol.
Ryan, D.G., and O'Neill, L.A.J. (2020). Krebs Cycle Reborn in Macrophage Immunometabolism. Annual review of immunology *38*, 289-313.
Sadiku, P., and Walmsley, S.R. (2019). Hypoxia and the regulation of myeloid cell metabolic imprinting: consequences for the inflammatory response. EMBO Rep *20*, e47388.
Schmid, M.C., Khan, S.Q., Kaneda, M.M., Pathria, P., Shepard, R., Louis, T.L., Anand, S., Woo, G., Leem, C., Faridi, M.H*., et al.* (2018). Integrin CD11b activation drives anti-tumor innate immunity. Nature communications *9*, 5379-5379.
Sender, R., and Milo, R. (2021). The distribution of cellular turnover in the human body. Nature Medicine *27*, 45-48.
Stanford, J.C., Young, C., Hicks, D., Owens, P., Williams, A., Vaught, D.B., Morrison, M.M., Lim, J., Williams, M., Brantley-Sieders, D.M*., et al.* (2014). Efferocytosis produces a prometastatic landscape during postpartum mammary gland involution. The Journal of Clinical Investigation *124*, 4737-4752.
Stritesky, G.L., Xing, Y., Erickson, J.R., Kalekar, L.A., Wang, X., Mueller, D.L., Jameson, S.C., and Hogquist, K.A. (2013). Murine thymic selection quantified using a unique method to capture deleted T cells. Proceedings of the National Academy of Sciences of the United States of America *110*, 4679-4684.
Taylor, C.T., and Colgan, S.P. (2017). Regulation of immunity and inflammation by hypoxia in immunological niches. Nature Reviews Immunology *17*, 774-785.
Thorp, E., Vaisar, T., Subramanian, M., Mautner, L., Blobel, C., and Tabas, I. (2011). Shedding of the Mer tyrosine kinase receptor is mediated by ADAM17 protein through a pathway involving reactive oxygen species, protein kinase Cδ, and p38 mitogen-activated protein kinase (MAPK). The Journal of biological chemistry *286*, 33335-33344.
Trayhurn, P. (2019). Oxygen-A Critical, but Overlooked, Nutrient. Front Nutr *6*, 10-10.
Trzeciak, A., Wang, Y.-T., and Perry, J.S.A. (2021). First we eat, then we do everything else: The dynamic metabolic regulation of efferocytosis. Cell Metabolism.
Viaud, M., Ivanov, S., Vujic, N., Duta-Mare, M., Aira, L.-E., Barouillet, T., Garcia, E., Orange, F., Dugail, I., Hainault, I*., et al.* (2018). Lysosomal Cholesterol Hydrolysis Couples Efferocytosis to Anti-Inflammatory Oxysterol Production. Circulation research *122*, 1369-1384.
Wang, B., Li, Q., Qin, L., Zhao, S., Wang, J., and Chen, X. (2011). Transition of tumor-associated macrophages from MHC class II(hi) to MHC class II(low) mediates tumor progression in mice. BMC Immunol *12*, 43.
Wang, G.G., Calvo, K.R., Pasillas, M.P., Sykes, D.B., Häcker, H., and Kamps, M.P. (2006). Quantitative production of macrophages or neutrophils ex vivo using conditional Hoxb8. Nature Methods *3*, 287.

Wang, Y., Subramanian, M., Yurdagul, A., Barbosa-Lorenzi, V.C., Cai, B., de Juan-Sanz, J., Ryan, T.A., Nomura, M., Maxfield, F.R., and Tabas, I. (2017). Mitochondrial Fission Promotes the Continued Clearance of Apoptotic Cells by Macrophages. Cell *171*, 331-345.e322.
Werfel, T.A., Elion, D.L., Rahman, B., Hicks, D.J., Sanchez, V., Gonzales-Ericsson, P.I., Nixon, M.J., James, J.L., Balko, J.M., Scherle, P.A*., et al.* (2019). Treatment-Induced Tumor Cell Apoptosis and Secondary Necrosis Drive Tumor Progression in the Residual Tumor Microenvironment through MerTK and IDO1. *79*, 171-182.
Williams, J.F., Blackmore, P.F., and Arora, K.K. (1985). The significance of sedoheptulose 1,7-bisphosphate in the metabolism and regulation of the pentose pathway in liver. Biochemistry international *11*, 599-610.
Wilson, J.L., Mayr, H.K., and Weichhart, T. (2019). Metabolic Programming of Macrophages: Implications in the Pathogenesis of Granulomatous Disease. Frontiers in immunology *10*, 2265-2265.
Yuan, Z.-Y., Luo, R.-Z., Peng, R.-J., Wang, S.-S., and Xue, C. (2014). High infiltration of tumor-associated macrophages in triple-negative breast cancer is associated with a higher risk of distant metastasis. Onco Targets Ther *7*, 1475-1480.
Yurdagul, A., Subramanian, M., Wang, X., Crown, S.B., Ilkayeva, O.R., Darville, L., Kolluru, G.K., Rymond, C.C., Gerlach, B.D., Zheng, Z*., et al.* (2020). Macrophage Metabolism of Apoptotic Cell-Derived Arginine Promotes Continual Efferocytosis and Resolution of Injury. Cell Metabolism *31*, 518-533.e510.
Yvan-Charvet, L., Pagler, T.A., Seimon, T.A., Thorp, E., Welch, C.L., Witztum, J.L., Tabas, I., and Tall, A.R. (2010). ABCA1 and ABCG1 Protect Against Oxidative Stress–Induced Macrophage Apoptosis During Efferocytosis. *106*, 1861-1869.
Zago, G., Saavedra, P.H.V., Keshari, K.R., and Perry, J.S.A. (2021). Immunometabolism of Tissue-Resident Macrophages – An Appraisal of the Current Knowledge and Cutting-Edge Methods and Technologies. Frontiers in Immunology *12*.
Zhang, S., Weinberg, S., DeBerge, M., Gainullina, A., Schipma, M., Kinchen, J.M., Ben-Sahra, I., Gius, D.R., Yvan-Charvet, L., Chandel, N.S*., et al.* (2019). Efferocytosis Fuels Requirements of Fatty Acid Oxidation and the Electron Transport Chain to Polarize Macrophages for Tissue Repair. Cell Metabolism *29*, 443-456.e445.

Figure 1: Chronic hypoxia enhances macrophage efferocytosis

(A) Efferocytosis by macrophages differentiated in the same O_2 environment, conditioned in standard O_2 or hypoxia. (Left) ER-Hoxb8 macrophage progenitors were differentiated under standard (21%) O_2 for 6 days. The macrophages were then replated and conditioned for 7 days in 21% O_2 (Std), 1% O_2 (Chr) or 7 days in 21% O_2 followed by 3h in 1% O_2 (Acu). (Right) Conditioned macrophages were co-cultured with CypHer5E-labeled apoptotic MDA-MB-231 cells at a 1:1 ratio for 1h. Efferocytosis was assessed via FACS. Data are from four independent experiments. Data are shown as mean ± SEM. ****p < .0001.

(B) Efferocytosis by standard oxygen- or hypoxia-conditioned macrophages of different apoptotic targets. Standard or chronic hypoxia-conditioned macrophages as in (A) were co-cultured with CypHer5E-labeled apoptotic cells at a 1:1 ratio. The following target types were used: Jurkat T cells, BrM2s, MDA-MD-231s, E0771s, and primary thymocytes. Efferocytosis was assessed via FACS. Data are from three independent experiments. Data are shown as mean ± SEM. ****p < .0001.

(C) Efferocytosis by macrophages differentiated in different O_2 levels. (Left) ER-Hoxb8 progenitors were differentiated under standard O_2 (21%) or hypoxia (1%) for 6d. Then, macrophages were replated and maintained in either 21% O_2 (Std) or 1% O_2 (Chr) for 7d. (Right) Macrophages were co-cultured with CypHer5E-labeled apoptotic MDA-MB-231 at a 1:1 ratio for 1h. Efferocytosis was assessed via FACS. Data are from three independent experiments. Data are shown as mean ± SEM. ****p < .0001.

(D) Chronic hypoxic conditioning promotes continual efferocytosis by macrophages. Conditioned macrophages as in (A) were first co-cultured with CFSE-labeled apoptotic MDA-MB-231 cells at a 1:1 ratio for 1h. Unengulfed apoptotic cells were removed by BMDM media wash (3x). Cells were rested for 1.5h, then co-cultured with CypHer5E-labeled apoptotic MDA-MB-231 cells at a 1:1 ratio for 1h and analyzed via FACS. Data are from three independent experiments. Data are shown as mean ± SEM. ****p < .0001.

(E, F) Time-lapse microscopy analysis of continual efferocytosis. (E) Macrophages were differentiated as in (A), replated in glass-bottom dishes, then conditioned in standard O_2 (21%) or hypoxia (1%) for 7d. Macrophages were co-cultured with DAPI (blue)/CypHer5E (pink)-labeled apoptotic Jurkat T cells at a 1:1 ratio. Imaging was started ~5-10min after the addition of apoptotic cells. Yellow arrows indicate newly engulfed apoptotic cells. (F) Quantification of the number of CypHer5E+ events (top) and the rate of degradation of engulfed apoptotic cells (bottom). For quantification, 115 efferocytotic macrophages from 8 standard oxygen scenes and 155 efferocytotic macrophages from 6 chronic hypoxia scenes were analyzed. Data were binned as number of events per cell and presented as a fraction of 100%. For analysis of degradation rate, 21 (standard oxygen) and 25 (chronic hypoxia) efferocytotic macrophages were analyzed. Time to degradation was defined as the time it takes to shrink an internalized corpse 50% after initial acidification (CypHer5E+).

(G, H) Low oxygen environment supports enhanced efferocytosis by splenic- and bone marrow-resident macrophages. Bone marrow (G) or spleen (H) were harvested from 7-week-old female C57BL/6J mice. Cells were isolated in a hypoxia chamber at 1% oxygen and seeded in either 1% or 21% oxygen overnight. Adherent macrophages were then co-cultured with CypHer5E-labeled apoptotic MDA-MD-231 cells at a 1:1 ratio for 1h. Efferocytosis was assessed via FACS. Data are from four independent experiments. Data are shown as mean ± SEM. ****$p < .0001$.

Figure 1: Chronic hypoxia enhances macrophage efferocytosis

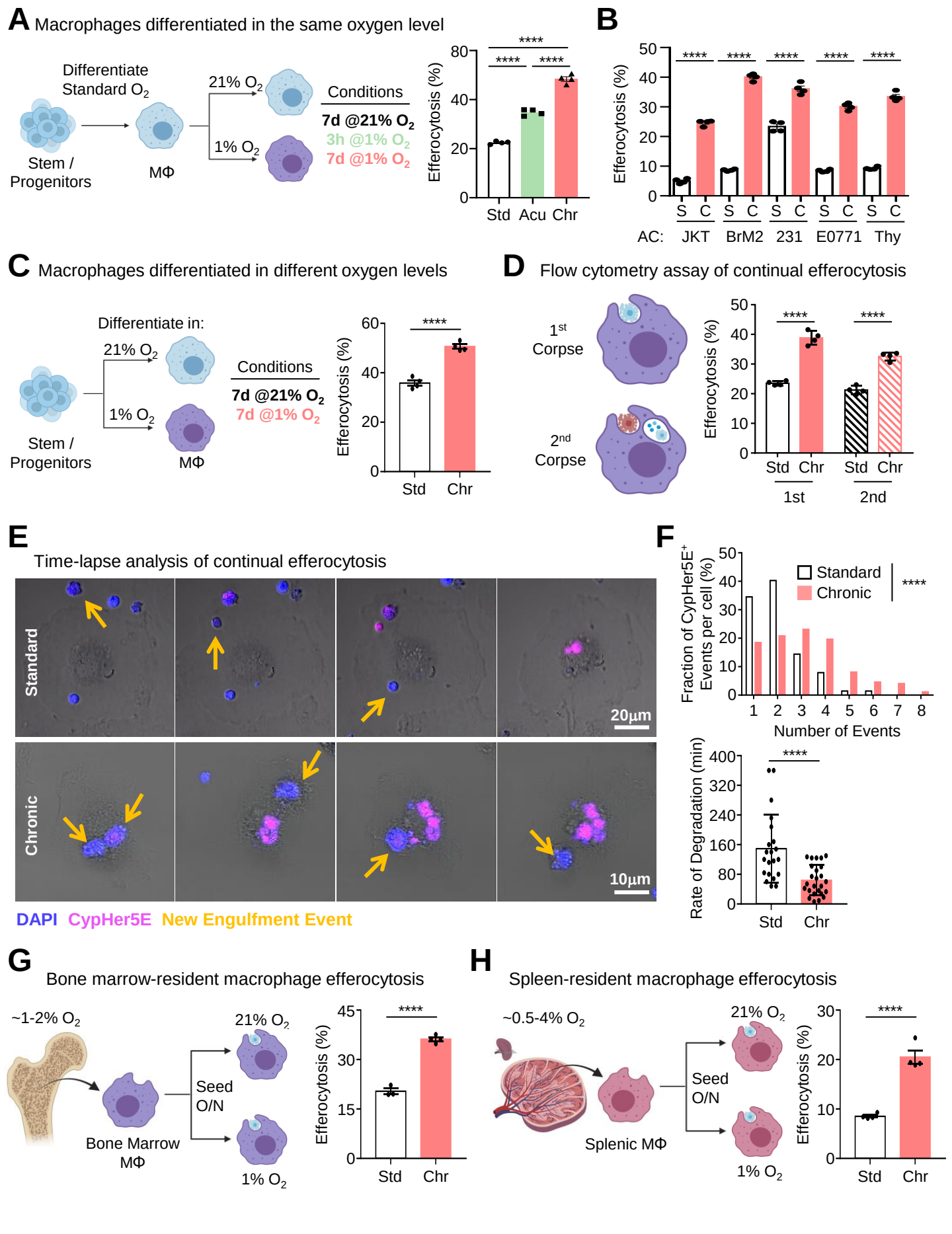

Figure S1: Chronic hypoxia enhances macrophage efferocytosis

(A) UV-induced apoptosis in different targets. Apoptosis was induced in MDA-MB-231s, BrM2s, and Jurkat T cells via UV-C irradiation and monitored for cell death at the time points indicated. (Left) Representative FACS plots of apoptosis as assessed using Annexin V (AV) and 7AAD. (Right) Quantification of AV^+7AAD^+, AV^+, $7AAD^+$, DN^+ (double negative) at different time points for each target cell. Data represent three experimental replicates. Data shown as mean ± SEM.

(B) Efferocytosis by standard oxygen- or hypoxia-conditioned macrophages of primary thymocytes treated with dexamethasone. Standard or chronic hypoxia-conditioned ER-Hoxb8 macrophages as in (**Figure 1A**) were co-cultured with CypHer5E-labeled apoptotic primary thymocytes at a 1:1 ratio. Instead of UV-C, cell death was induced using dexamethasone. Efferocytosis was assessed via FACS. Data are from four independent experiments. Data are shown as mean ± SEM. ****p < .0001.

(C, D) Efferocytosis by standard oxygen- or hypoxia-conditioned bone marrow-derived macrophages of primary thymocytes treated with UV-C or dexamethasone. Standard or chronic hypoxia-conditioned bone marrow-derived macrophages were co-cultured with CypHer5E-labeled apoptotic primary thymocytes at a 1:1 ratio. Cell death was induced using UV-C (C) or dexamethasone (D). Efferocytosis was assessed via FACS. Data are from four independent experiments. Data are shown as mean ± SEM. ****p < .0001.

(E) FACS assessment of efferocytotic capacity. Conditioned macrophages were co-cultured with TAMRA-labeled apoptotic MDA-MB-231 cells at a 1:1 ratio for 1h and analyzed for efferocytosis. (Left) TAMRA+ percentage and (Right) TAMRA geometric mean of efferocytotic standard oxygen- and chronic hypoxia-conditioned macrophages. Data represent three independent experiments. Data shown as mean ± SEM. ****p < .0001; ns = not significant.

(F) Gating strategy for experiments in Figure 1G and 1H. Tissue-resident macrophages were gated as $CD11b^{high}$ $F4/80^{high}$ and analyzed for CypHer5E.

(G) HIF-1α and HIF-2α protein expression in standard, acute, and chronic hypoxia-conditioned macrophages. HIF-1α and HIF-2α protein expression was examined by FACS in macrophages conditioned as in **Figure 1A**.

(H) HIF-1α and HIF-2α protein expression at different time points during hypoxia conditioning. Macrophages were harvested on day 3, 5, and 7 of standard oxygen or hypoxia conditioning and examined for HIF-1α and HIF-2α protein expression by flow cytometry.

Figure S1: Chronic hypoxia enhances macrophage efferocytosis

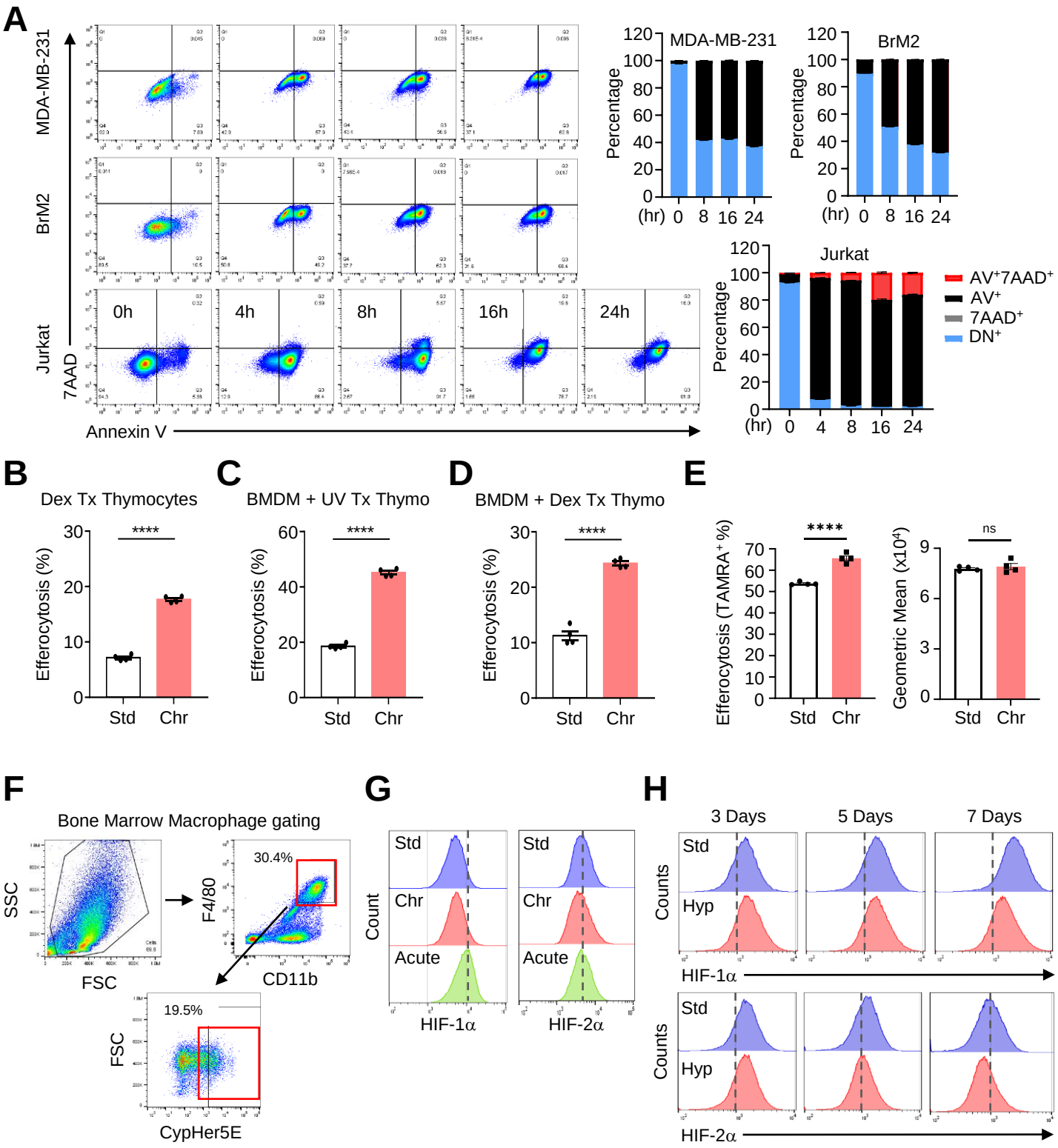

Figure 2: Macrophages adapt to chronic hypoxia

(A, B) RNA sequencing analysis of macrophages conditioned in different oxygen environments reveals regulation of novel functional programs in chronic hypoxia-conditioned macrophages. (A) Schematic of method used for RNA sequencing analysis. ER-Hoxb8 progenitors were differentiated under standard (21%) oxygen for 6d. Macrophages were then replated and conditioned for 7d in standard (21%) oxygen (Std), for 7d in hypoxia (1%; Chr), or in standard oxygen for 7d followed by 3h of hypoxia (Acu). Macrophages were lysed in the conditioned oxygen environments for cell and mRNA extraction. (B) We detected significant changes in 1,048 genes in chronic hypoxia-conditioned macrophages relative to standard oxygen-conditioned macrophages. Differentially expressed genes were classified according to known or putative (based on family or sequence similarity) function. Genes were considered significant if they met a false discovery rate-adjusted p value < .05. Three independent experiments were analyzed for each condition. ECM, extracellular matrix.

(C) Identification of transcripts uniquely induced by chronic hypoxia conditioning. Analysis of data from (A) to specifically identify transcripts differentially regulated in chronic hypoxia-conditioned macrophages compared to standard oxygen and acute hypoxia ('Chronic Hypoxia-Specific'), significantly differentially regulated under acute hypoxia and maintained during chronic conditioning ('General Hypoxia'), or transcripts that are only significantly differentially regulated in chronic hypoxia-conditioned macrophages compared to standard oxygen ('Chronic vs. Standard O_2 Only').

(D) Chronic hypoxia-conditioned macrophages express unique proteins and induce or suppress distinct functional programs. Experiments were performed as in (A) but instead analyzed via TMT-labeled mass spectrometry (proteomics). We detected significant changes in 1,591 proteins in chronic hypoxia-conditioned macrophages relative to standard oxygen-conditioned macrophages. Differentially expressed proteins were classified according to known or putative (based on family or sequence similarity) function. Proteins were considered significant if they met a false discovery rate-adjusted p value < .05. Six independent experiments were analyzed for each condition. MAPK, mitogen-activated protein kinase. OXPHOS, oxidative phosphorylation. Pathway significance was determined using Fisher's Exact Tests and presented as the negative log of the adjusted p value.

(E) Flow cytometric validation of selected differentially expressed genes/proteins. Macrophages were conditioned as in (A), then harvested and analyzed for Arginase 1 (Arg1), CD71, and 4-1BB expression by flow cytometry. Shown are representative FACS histograms and normalized mean fluorescence intensity (MFI). Data represent three independent experiments and are shown as mean ± SEM. *p < 0.05. ****p < .0001.

Figure 2: Macrophages adapt to chronic hypoxia

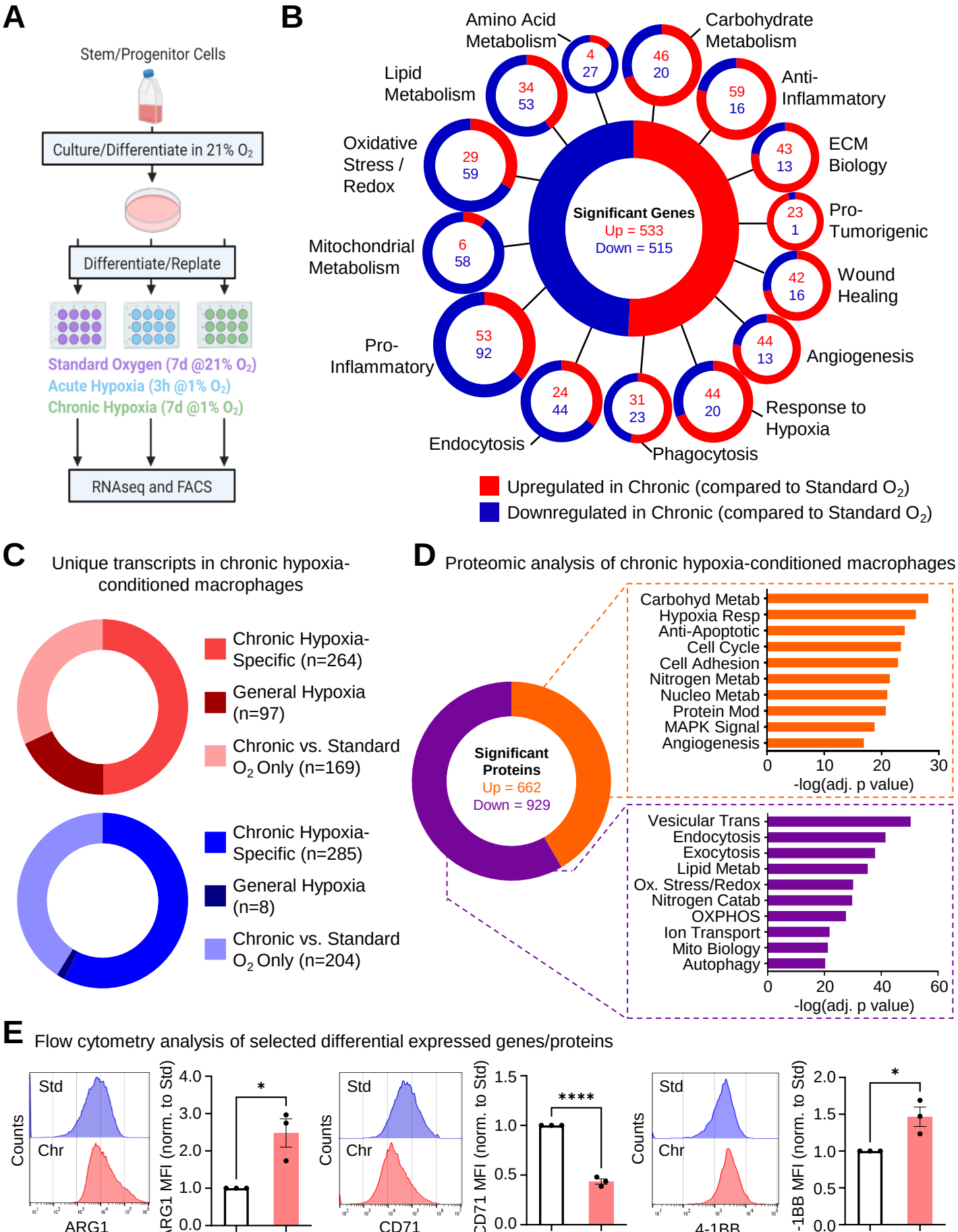

Figure S2: Macrophages adapt to chronic hypoxia

(A, B) Functional programs and general processes differentially regulated in chronic hypoxia-conditioned macrophages. Additional analyses of RNA sequencing data obtained, analyzed, and presented as in **Figure 1A**.

Figure S2. Macrophages adapt to chronic hypoxia

A

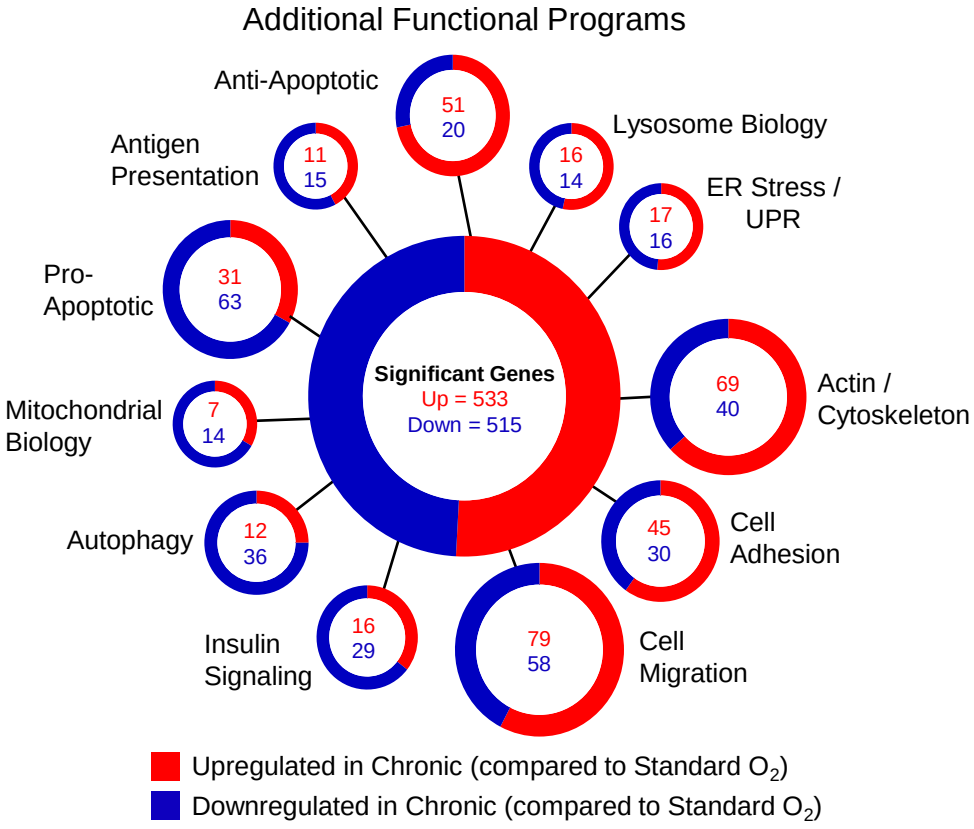

B

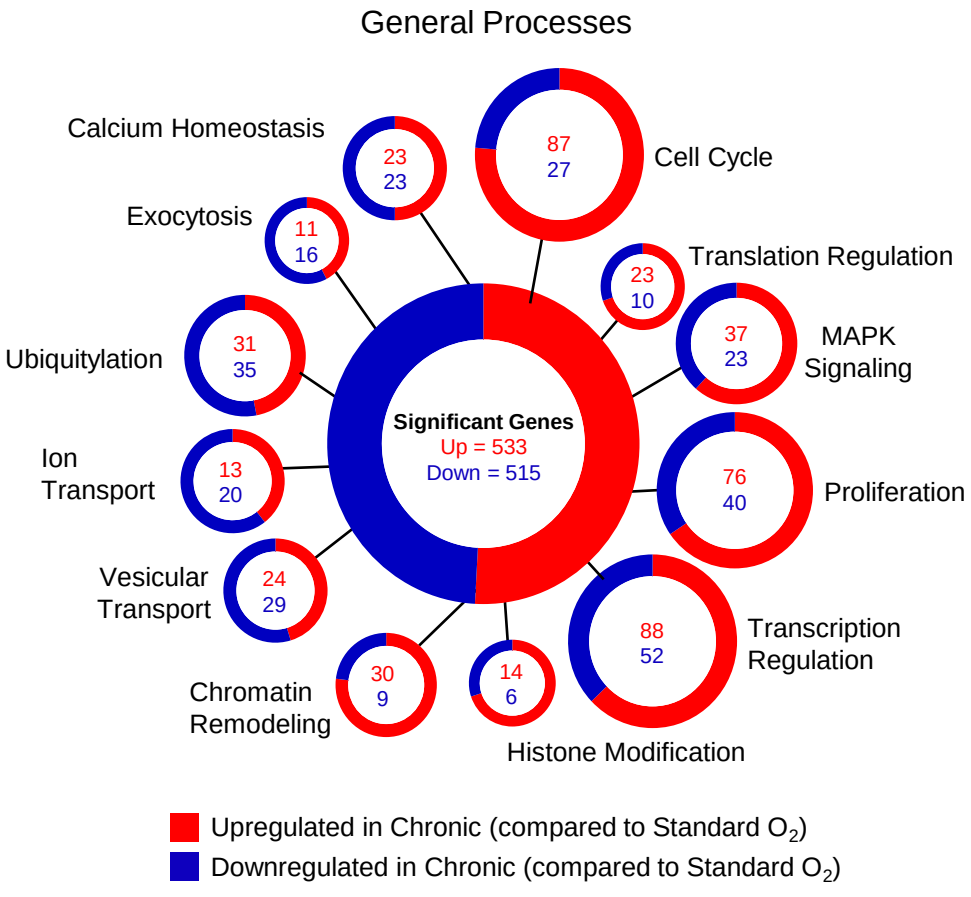

Figure 3: Chronic hypoxia induces a metabolic state poised for efficient efferocytosis

(A) Global proteomic analysis of naive and efferocytotic macrophages conditioned in standard oxygen or chronic hypoxia reveals 'primed' and 'poised' states. (Left) ER-Hoxb8 progenitors were differentiated and conditioned as in **Figure 1A**. Macrophages were subsequently co-cultured with apoptotic MDA-MB-231s that were labeled with ^{13}C-Lysine to an incorporation rate > 99%. Naïve and efferocytotic macrophages from standard oxygen and hypoxia conditions were harvested in the indicated oxygen environment prior to downstream processing and mass spectrometry analysis. Four independent experiments were analyzed for each condition. (Middle/Right) Based on our analyses of global proteomics data (see Figure S3), we observed differentially regulated mRNA transcripts (Core Programs; Middle) that were concomitantly differentially regulated at the protein level in naïve macrophages (Primed; Top Right) or differentially regulated mRNA transcripts that were not differentially regulated in naïve macrophages but instead were differentially regulated in efferocytotic macrophages (Poised; Bottom Right). Numbers represent individual genes/proteins differentially regulated, with light shading representing downregulated and dark shading representing upregulated.

(B) Representative genes/proteins of primed and poised states. Shown are representative transcripts/proteins from each state observed in **Figure 3A**. PFKL/*Pfkl*, ATP-dependent 6-phosphofructokinase, liver type. PLOD1/*Plod1*, Procollagen-lysine,2-oxoglutarate 5-dioxygenase 1.

Figure 3: Chronic hypoxia induces a metabolic state poised for efficient efferocytosis

A Chronic hypoxia-conditioned macrophage transcripts found in resting (primed) or efferocytotic (poised) macrophages

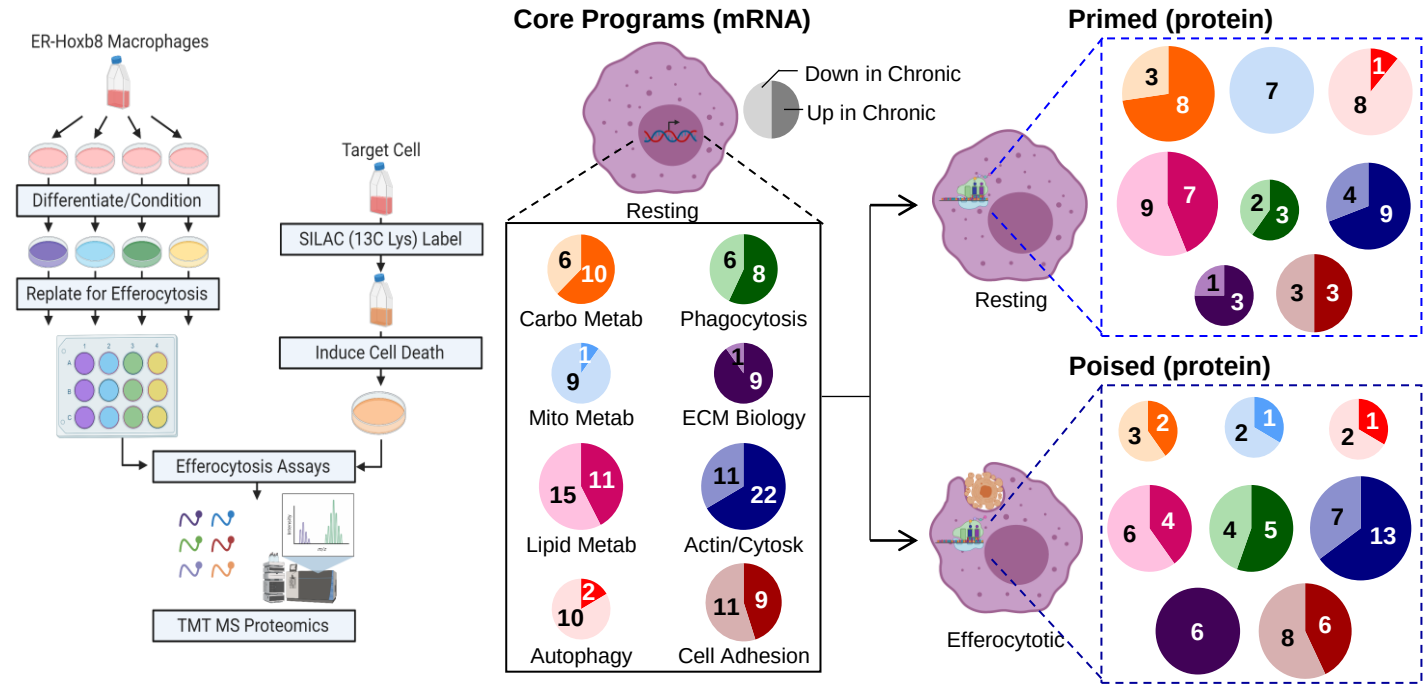

B

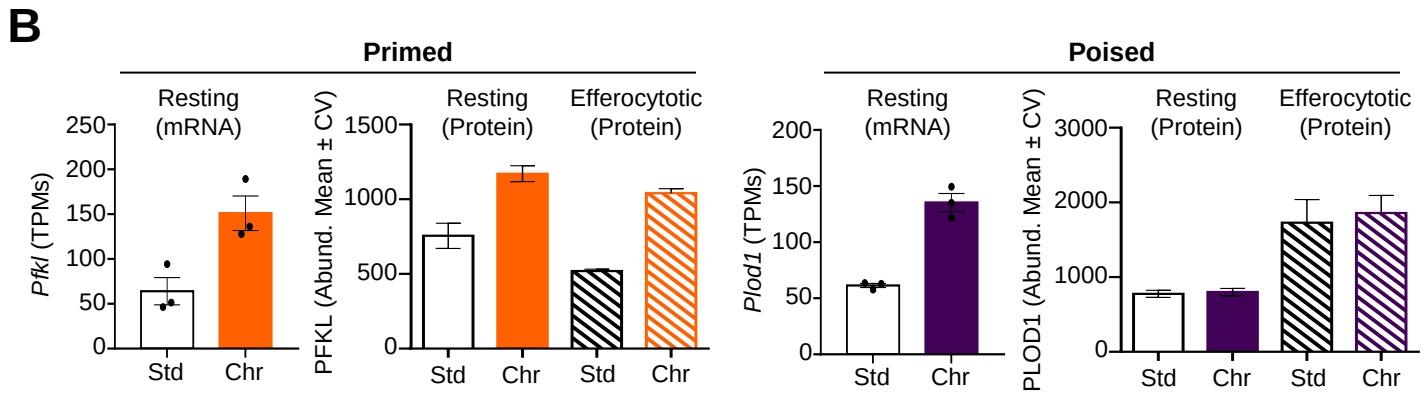

Figure S3: Chronic hypoxia induces a metabolic state poised for efficient efferocytosis

(A) Analysis of chronic hypoxia-conditioned macrophage transcripts also found via proteomics. Shown is the cross-reference analysis of RNA sequencing data from **Figure 2A** and global proteomic data from **Figure 2D**. (Top) Upregulated transcripts not detected in proteomics (orange), detected and found significantly upregulated in proteomics (red), or detected but found not significantly upregulated in proteomics (gray). (Bottom) Downregulated transcripts not detected in proteomics (purple), detected and found significantly downregulated in proteomics (blue), or detected but found not significantly downregulated in proteomics (gray).

(B) Global proteomic analysis of resting and efferocytotic macrophages in standard oxygen versus chronic hypoxia conditions. Shown are the number of differentially up- or downregulated proteins in comparisons between naïve and efferocytotic standard oxygen-conditioned macrophages (Top Left), between naïve and efferocytotic chronic hypoxia-conditioned macrophages (Top Right), and between efferocytotic standard oxygen and hypoxia-conditioned macrophages (Bottom).

(C) Functional program analysis of resting and efferocytotic macrophages in standard oxygen versus chronic hypoxia conditions. Similar to analyses in Figure 2D, shown are functional program analyses of differentially expressed proteins from comparisons shown in Figure S3B.

Figure S3: Chronic hypoxia induces a metabolic state poised for efficient efferocytosis

Figure 4: Mapping metabolic pathway use in chronic hypoxia-conditioned macrophages

(A) Network analysis of differentially expressed metabolic transcripts identified in chronic hypoxia-conditioned macrophages. Metabolic genes that are differentially regulated in chronic hypoxia-conditioned macrophages (**Figure 2**) are represented using network analysis to determine family clusters (shaded areas) and connectedness between individual genes.

(B) Consumption of glucose and release of lactate by standard oxygen and hypoxia-conditioned macrophages. Macrophages were differentiated and cultured as in **Figure 1A**. Media was replaced on days 2, 4, and 6, and harvested 24h later (e.g., on days 3, 5, and 7). Media was analyzed using a 2950D Biochemistry Analyzer (YSI Life Sciences) for glucose and lactate levels compared relative to media controls conditioned in parallel. Two independent experiments were analyzed for each condition, with 4 biological replicates per experiment. Data are shown as mean ± SEM. ****$p < .0001$.

(C) Unique metabolomic profile in chronic hypoxia-conditioned macrophages. Macrophages were differentiated and conditioned as in **Figure 1A** then isolated for untargeted metabolomic analysis. (Left) upregulated and (Right) downregulated pathways in chronic hypoxia-conditioned macrophages relative to standard oxygen and acute hypoxia-conditioned macrophages are shown (see Figure S4B for principal component analysis of all three conditions). Three independent experiments were performed for each condition.

(D) Individual metabolites from untargeted metabolomics analysis. Shown are representative metabolites from significantly differentially regulated pathways from **Figure 4C**, specifically upper glycolysis (blue) and pentose phosphate pathway (PPP, purple). See also Figure S4C for additionally representative metabolites from upper glycolysis, PPP, lower glycolysis/TCA cycle (orange), and alanine/aspartate/glutamine metabolism (Ala, Asp, Glu Metabolism, gray). Data are shown as mean ± SEM. All metabolites are significant, $p < .0001$. G6P, glucose 6-phosphate. F6P, fructose 6-phosphate. 6-PGDL, 6-phosphogluconolactone. 6-PG, 6-phosphogluconate. E4P, erythrose 4-phosphate. S7P, sedoheptulose 7-phosphate.

Figure 4: Mapping metabolic pathway use in chronic hypoxia-conditioned macrophages

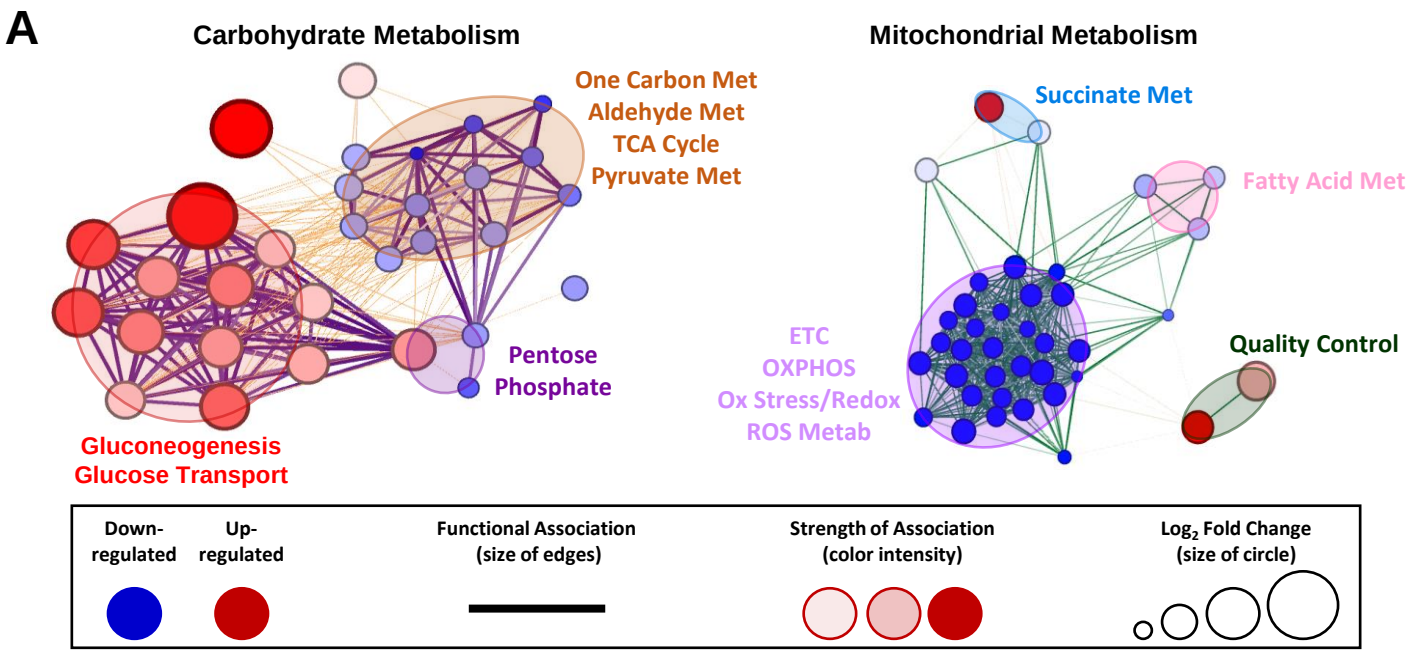

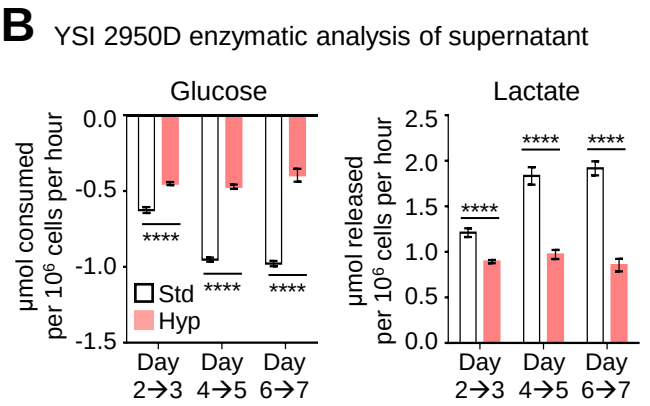

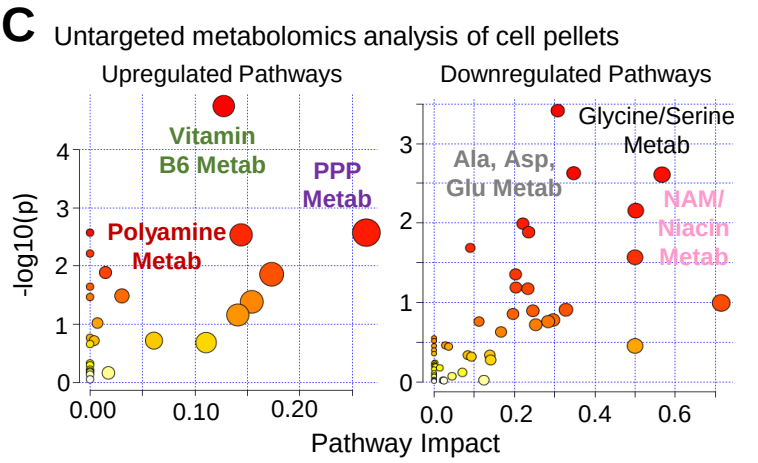

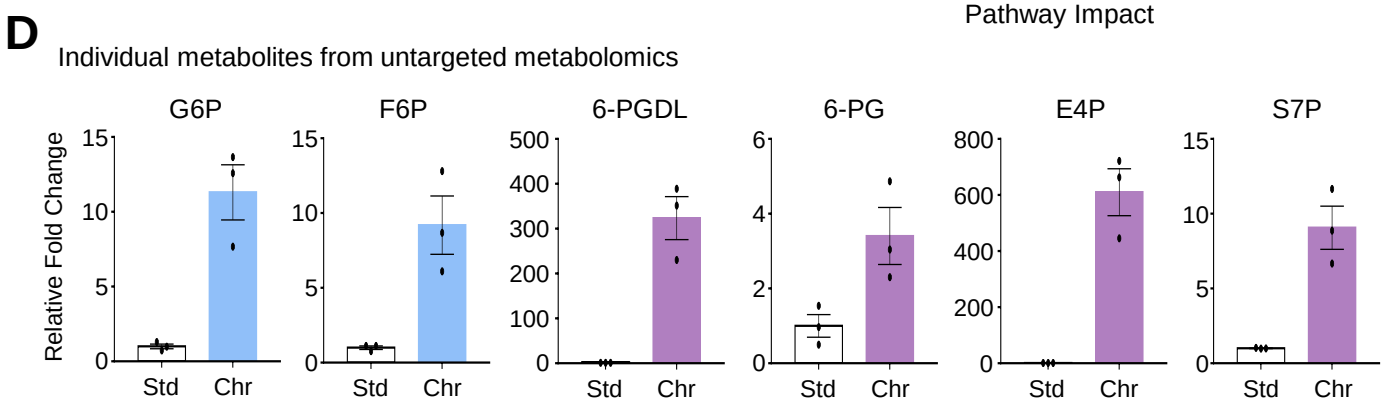

Figure S4: Mapping metabolic pathway use in chronic hypoxia-conditioned macrophages

(A) Network analysis of differentially expressed metabolic transcripts identified in chronic hypoxia-conditioned macrophages. Analyses performed as in **Figure 4A**. Metabolic genes that are differentially regulated in chronic hypoxia-conditioned macrophages (**Figure 2**) are represented using network analysis to determine family clusters (shaded areas) and connectedness between individual genes.

(B) Principal components analysis of untargeted metabolomics analysis of standard oxygen and hypoxia-conditioned macrophages. Shown is a principal components analysis (PCA) of experiments performed in **Figure 4C**. Principal component (PC) 1, which accounts for 74.3% of the total variance, is entirely accounted for by chronic hypoxia-conditioned macrophages, whereas PC2 (12.4% of total variance) represents the acute hypoxia vs standard oxygen comparison.

(C) Individual metabolites from untargeted metabolomics analysis. As in **Figure 4D**, shown are representative metabolites from significantly differentially regulated pathways from **Figure 4C**, specifically upper glycolysis (blue), pentose phosphate pathway (purple), lower glycolysis/TCA cycle (orange), and alanine/aspartate/glutamine metabolism (gray). Data are shown as mean ± SEM. All metabolites except for pyruvate are significant, ranging from $p<.0001$ to $p<.05$. FBP, fructose 1,6-bisphosphate. R5P, ribose 5-phosphate. SAM, S-adenosyl methionine. SAH, S-adenosyl homocysteine. Glyc3P, glycerol 3-phosphate.

Figure S4: Mapping metabolic pathway use in chronic hypoxia-conditioned macrophages

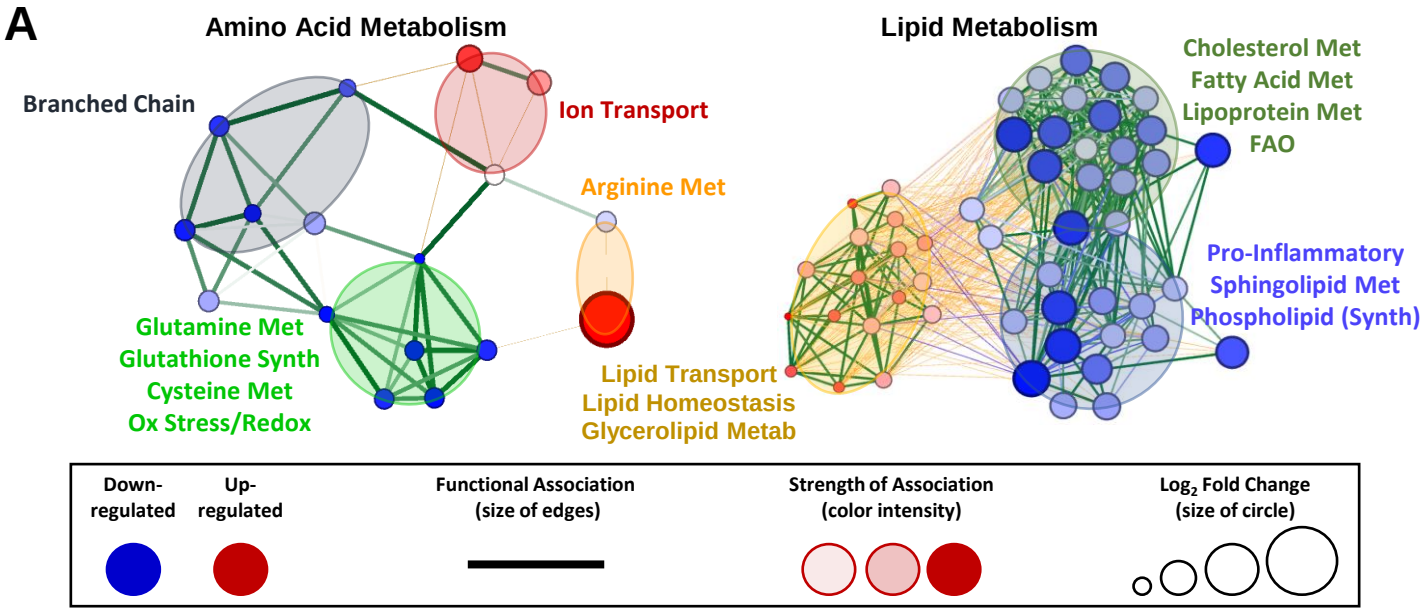

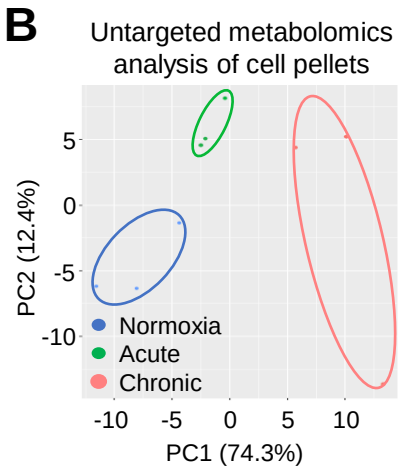

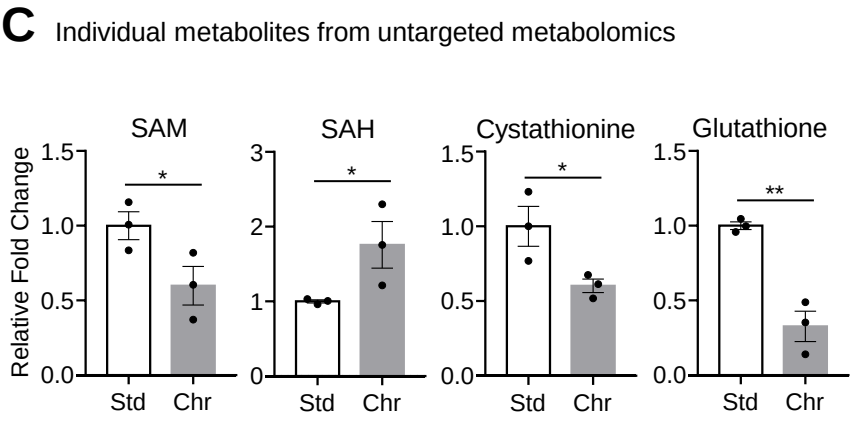

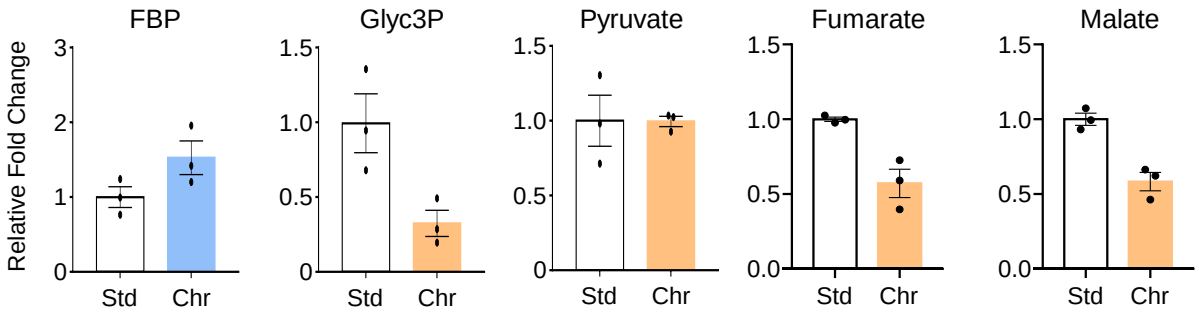

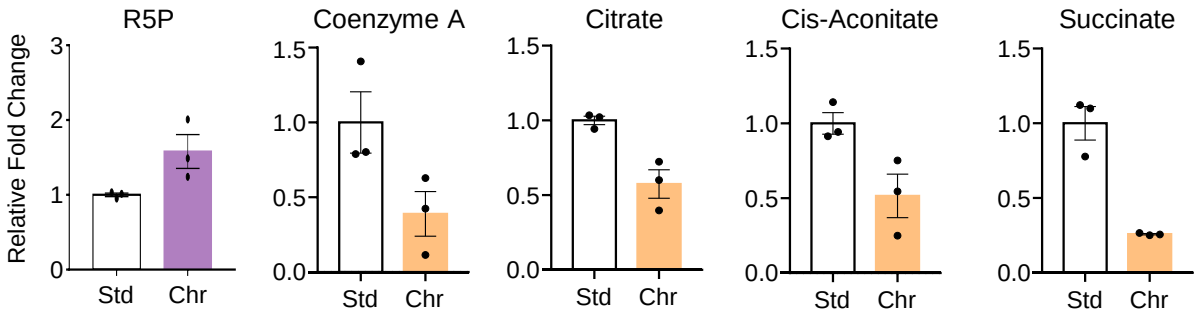

Figure 5: Macrophages co-opt noncanonical pentose phosphate loop for redox homeostasis

(A) The pentose phosphate pathway is active in chronic hypoxia-conditioned macrophages. (Left) Schematic for isotopologue analysis of intermediates for pentose phosphate pathway (PPP; M+1) and glycolysis (M+2) in [1,2-^{13}C]-glucose tracing experiments. (Right) Macrophages were differentiated and conditioned as in **Figure 1A**. On day 6, macrophages were cultured with media containing [1,2-^{13}C]-glucose for 16h then analyzed via LC-MS. M+1 G6P, which arises via gluconeogenesis, is denoted in green. PPP intermediates (M+1) are denoted in red and glycolysis intermediates (M+2) are denoted in blue. Shown is the fractional enrichment of the indicated isotopologues. For relative abundance, see Figure S5A. Three independent experiments were performed for each condition. Data are shown as mean ± SEM. **p < .01; ***p < .001; ****p < .0001; ns = not significant. G6P, glucose 6-phosphate. F6P, fructose 6-phosphate. FBP, fructose 1,6-bisphosphate. 3PG, 3-phosphoglyceric acid.

(B) Lactate is not a major product of glucose metabolism in chronic hypoxia-conditioned macrophages. (Left) Shown are representative peaks for PPP (M+1)- and glycolysis (M+2)-derived lactate in media analyzed via NMR from experiments performed similar to **Figure 5A**. (Right) Cumulative data of the M+1 lactate fraction from our NMR analysis of macrophage-conditioned media relative to cell-free conditioned media. Data are from four biological replicates. Data are shown as mean ± SEM. ****p < .0001.

(C) Identification of flux through novel pentose phosphate pathway intermediates in chronic hypoxia-conditioned macrophages. Analysis of experiments performed in **Figure 5A**. Shown is summary data from our identification of isotopologues arising via gluconeogenesis (green). Additionally, we identified flux through the novel metabolite sedoheptulose 1,7-bisphosphate. Shown is the relative abundance of the indicated isotopologues. For fractional enrichment, see Figure S5B. Three independent experiments were analyzed for each condition. Data shown as mean ± SEM. *p < .05; **p < .01; ***p < .001; ****p < .0001. G6P, glucose 6-phosphate. S7P, sedoheptulose 7-phosphate. 3PG, 3-phosphoglyceric acid. F6P, fructose 6-phosphate. FBP, fructose 1,6-bisphosphate.

(D) Gluconeogenesis is prevalent in chronic hypoxia-conditioned macrophages. (Top) Schematic for [U-^{13}C]-glucose flux analysis including routes through glycolysis, PPP, and gluconeogenesis. (Bottom) Experiments were performed identical to **Figure 5A**, except macrophages were incubated with [U-^{13}C]-glucose for 16h then analyzed via LC-MS. M+3 G6P, which arises via PPP, is denoted in red. M+3 F6P, which arises via gluconeogenesis, is denoted in green. M+3 lactate, which arises via conventional glycolysis, is denoted in blue. Shown is the relative abundance of the indicated isotopologues. For fractional enrichment, see Figure S5C. Three independent experiments were performed for each condition. Data are shown as mean ± SEM. *p < .05; **p < .01; ***p < .001. G6P, glucose 6-phosphate. F6P, fructose 6-phosphate.

(E) Less glucose enters the TCA cycle in chronic hypoxia-conditioned macrophages. Data are from experiments performed in **Figure 5D**. Glucose entry into the TCA cycle can occur via citrate (M+2)

or oxaloacetate (M+3). Shown is the relative abundance of the indicated isotopologues. For fractional enrichment, see Figure S5E. Three independent experiments were performed for each condition. Data shown as mean ± SEM. *p < .05; **p < .01.

(F) NADPH synthesis is enhanced in chronic hypoxia-conditioned macrophages. (Left) Schematic of NADPH synthesis via pentose phosphate pathway. Macrophages were differentiated and conditioned as in **Figure 5A**. (Center) NADPH levels (pmol) were quantified relative to media-only controls and the ratio of $NADP^+$/NADPH was calculated and plotted relative to standard oxygen-conditioned macrophages (Right). Three independent experiments were analyzed for each condition. Data shown as mean ± SEM. *p < .05; ****p < .0001.

(G) Chronic hypoxia-conditioned macrophages exhibit lower lipid peroxidation compared to standard oxygen-conditioned macrophages. Macrophages were differentiated and conditioned as in **Figure 5A**, incubated with C11-BODIPY 581/591 and analyzed via flow cytometry. Shown are representative FACS plots (Left) and fold change of lipid peroxidation level normalized to standard oxygen-conditioned macrophages. Data are representative of three independent experiment per condition. Data are presented as mean ± SEM. *p < .05.

Figure 5: Macrophages co-opt noncanonical pentose phosphate loop for redox homeostasis

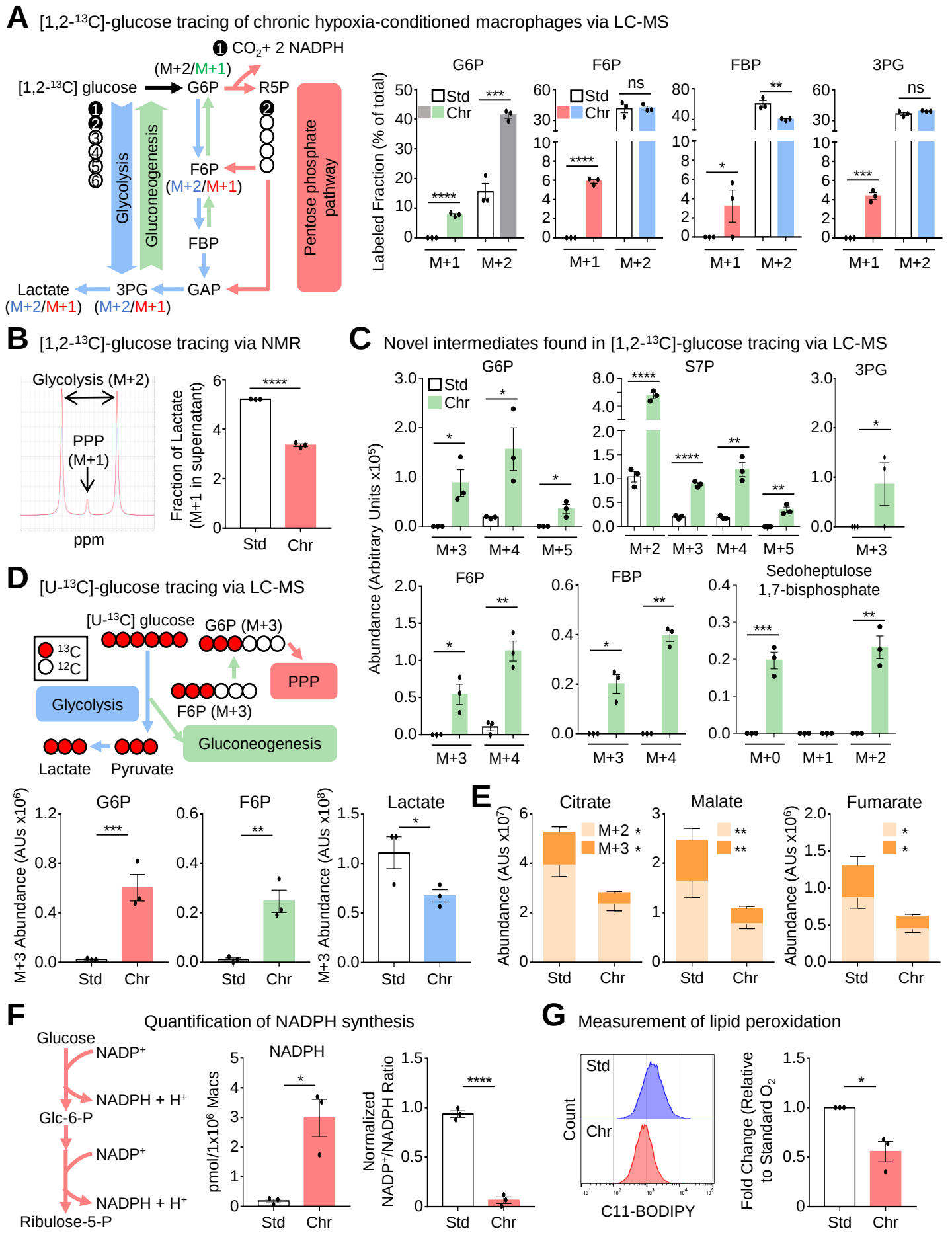

Figure S5: Macrophages co-opt noncanonical pentose phosphate loop for redox homeostasis

(A) The pentose phosphate pathway is active in chronic hypoxia-conditioned macrophages. (Left) Data from experiments performed in **Figure 5A**. Shown is the relative abundance of the indicated isotopologues. Intermediates from PPP are denoted in red, gluconeogenesis denoted in green, conventional glycolysis denoted in blue, and TCA cycle denoted in orange. For fractional enrichment, see **Figure 5A**. Three independent experiments were performed for each condition. Data shown as mean ± SEM. *p < .05; **p < .01; ***p < .001; ****p < .0001. G6P, glucose 6-phosphate. F6P, fructose 6-phosphate. FBP, fructose 1,6-bisphosphate. 3PG, 3-phosphoglyceric acid. PEP, phosphoenolpyruvate. S7P, sedoheptulose 7-phosphate.

(B) Identification of flux through novel pentose phosphate pathway intermediates in chronic hypoxia-conditioned macrophages. Data from experiments performed in **Figure 5A**. Shown is the fractional enrichment of the indicated isotopologues from **Figure 5C**. Gluconeogenesis intermediates are denoted in green. Three independent experiments were analyzed for each condition. Data shown as mean ± SEM. *p < .05; **p < .01; ***p < .001; ****p < .0001; ns = not significant. G6P, glucose 6-phosphate. S7P, sedoheptulose 7-phosphate. F6P, fructose 6-phosphate. FBP, fructose 1,6-bisphosphate. 3PG, 3-phosphoglyceric acid.

(C) Gluconeogenesis is prevalent in chronic hypoxia-conditioned macrophages. Data from experiments performed in **Figure 5D**. (Left) Shown is the fractional enrichment of glucose across all identified isotopologues, suggesting that no new glucose was formed via gluconeogenesis. (Right) Shown is the fractional enrichment of the indicated isotopologues from **Figure 5D**. PPP intermediates are denoted in red, gluconeogenesis in green, and conventional glycolysis in blue. Three independent experiments were performed for each condition. Data are shown as mean ± SEM. *p < .05; ***p < .001.

(D) Less glucose is converted to alanine in chronic hypoxia-conditioned macrophages. Abundance (Left) and labeled fraction (Right) of M+3 alanine from experiments performed in **Figure 5D**. Three independent experiments were performed for each condition. Data are shown as mean ± SEM. ***p < .001; ns = not significant.

(E) Less glucose enters the TCA cycle in chronic hypoxia-conditioned macrophages. (Left) Labeled fraction of TCA cycle intermediates identified in experiments performed in **Figure 5D** and presented in **Figure 5E**. Three independent experiments were performed for each condition. Data shown as mean ± SEM. *p < .05.

(F) Less glucose contributes to nucleotide synthesis in chronic hypoxia-conditioned macrophages. The ^{12}C and ^{13}C abundance of IMP (Top) and GMP (Bottom) from experiments performed in **Figure 5D**. Three independent experiments were performed for each condition. Data are shown as mean ± SEM. *p < .05; **p < .01; ***p < .001.

Figure S5: Macrophages coopt noncanonical pentose phosphate loop for redox homeostasis

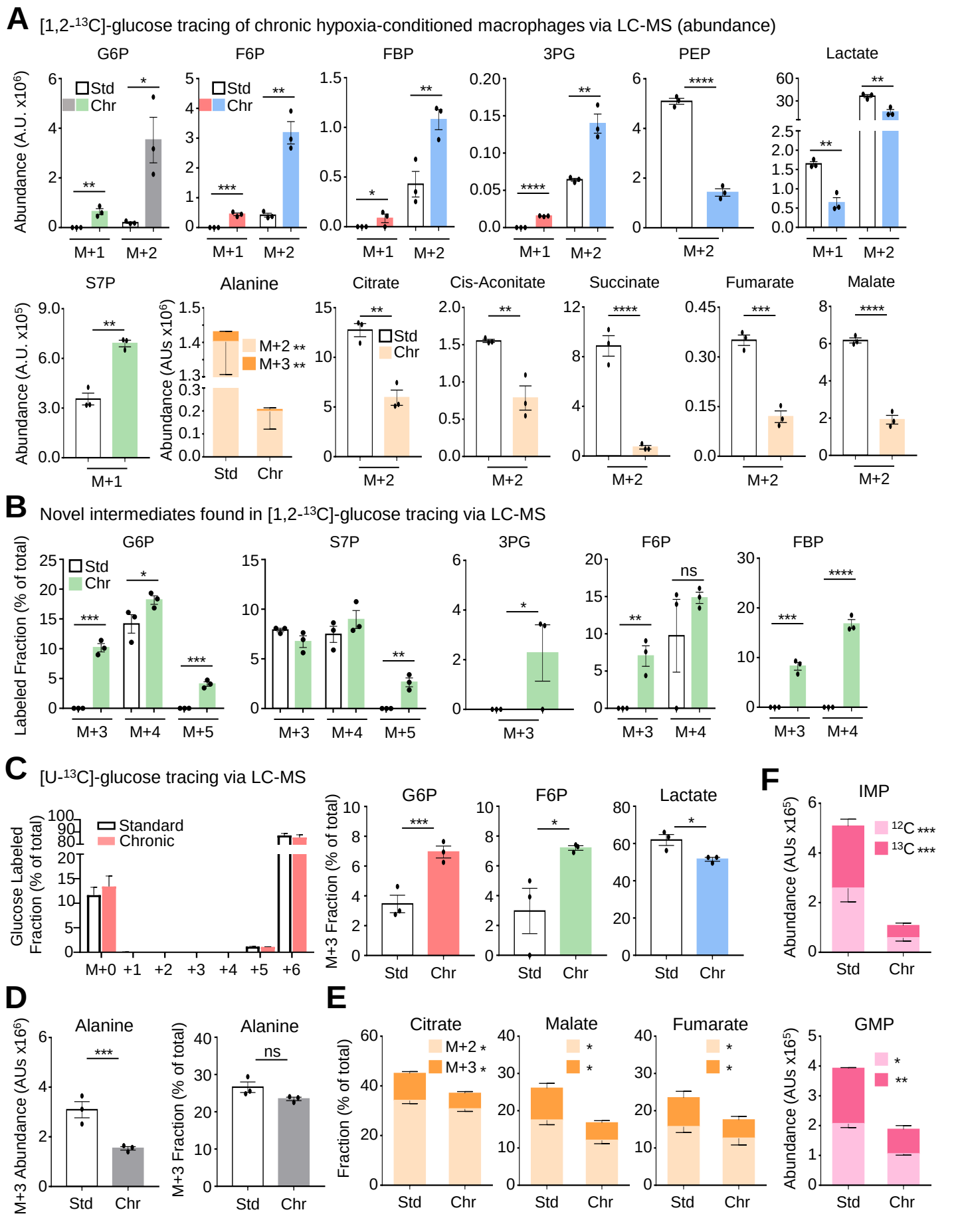

Figure S6: Macrophages co-opt noncanonical pentose phosphate loop for redox homeostasis

(A) $NADP^+$ levels in standard oxygen and chronic hypoxia-conditioned macrophages. Data are from experiments performed as in **Figure 5F**. Three independent experiments were performed for each condition. Data are shown as mean ± SEM. ns = not significant.

(B) Analysis of total cellular oxidative stress levels in conditioned macrophages. Macrophages were differentiated and conditioned as in **Figure 1A**. Oxidative stress levels were measured by labeling macrophages with CellRox Deep Red (ThermoFisher) and analysis via flow cytometry. Shown are representative FACS plots (Left) and summary plots of the MFI fold change relative to standard oxygen-conditioned macrophages (Right). Data are representative of three independent experiments per condition. Data are shown as mean ± SEM. **p < .01.

(C-F) Mitochondrial membrane potential (MMP) and mitochondrial mass of conditioned macrophages. Macrophages were differentiated and conditioned as in **Figure 1A** and labeled with Mitotracker Deep Red (C and D for MMP) or Mitotracker Green (E and F for mitochondrial mass). Macrophages were subsequently analyzed by fluorescence confocal microscopy (Left) or flow cytometry (Right). For microscopy, images are representative of one biological replicate. For FACS analysis, plots represent two biological experiments which are summarized as the MFI fold change relative to standard oxygen-conditioned macrophages. Data shown as mean ± SEM.

(G) Mitochondrial ROS levels in conditioned macrophages. Macrophages were differentiated and conditioned as in **Figure 1A**, labeled with MitoSox Red, and analyzed via flow cytometry. Shown are representative FACS plots (Left) and summary plots of the MFI fold change relative to standard oxygen-conditioned macrophages (Right). Data are representative of three independent experiments per condition. Data are shown as mean ± SEM. ****p < .0001.

(H) Total glutathione, GSH, GSSG, and oxidized/reduced glutathione ratio in conditioned macrophages. Macrophages were differentiated and conditioned as in **Figure 1A**. Cells were subsequently analyzed via plate reader. Net relative luminescence unit (RLU) values were normalized to cell number. GSH/GSSG ratios were normalized to standard oxygen-conditioned macrophages. Data are from four independent experiments for each condition. Data are shown as mean ± SEM. **p< .01; ***p< .001.

Figure S6: Macrophages coopt noncanonical pentose phosphate loop for redox homeostasis

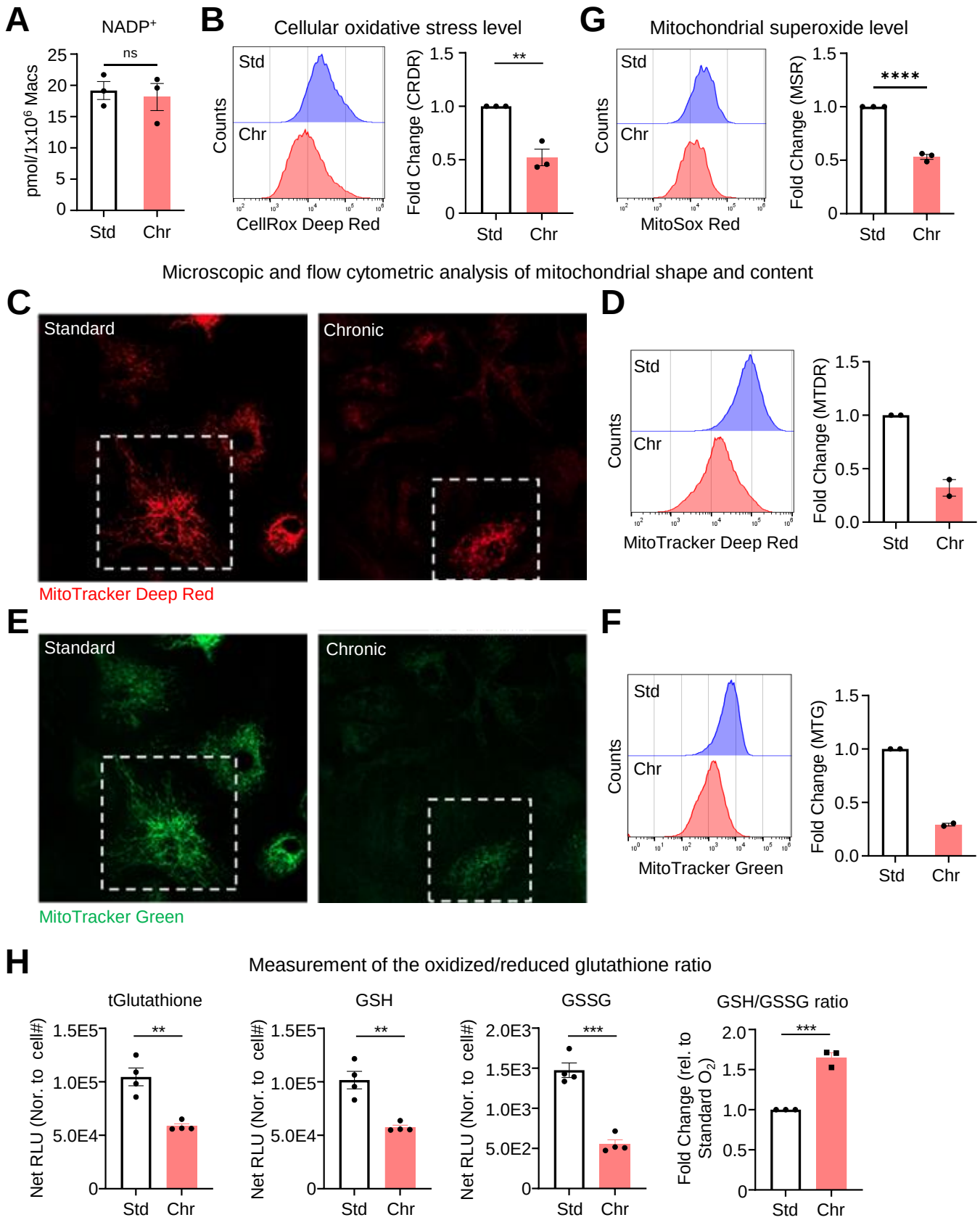

Figure 6: Noncanonical pentose phosphate loop supports continual efferocytosis

(A, B) Targeting PPP metabolism or gluconeogenesis reduces efferocytosis specifically in chronic hypoxia-conditioned macrophages. (A) Schematic illustrating the approaches used to target key PPP enzymes (G6PDi targeting G6PD and 6-AN targeting 6PGD) and gluconeogenesis (FBPi targeting FBP1 and exogenous lactate). (B) Macrophages were differentiated and conditioned as in **Figure 1A**. Indicated treatments (or vehicle controls) were added prior to the start of an assays. Macrophages were subsequently cultured with CypHer5E-labeled apoptotic MDA-MB-231s at a 1:1 ratio for 1h in the presence of indicated inhibitors (or vehicle controls). Efferocytosis was assessed via flow cytometry. Data are representative of three independent experiments. Data are shown as mean ± SEM. **p < .01; ***p < .001; ****p < .0001; ns = not significant.

(C) Disrupting PPP metabolism impairs continual efferocytosis in chronic hypoxia-conditioned macrophages. Macrophages were differentiated and conditioned as in **Figure 6B** then subsequently cultured with CFSE-labeled apoptotic MDA-MB-231 cells at a 1:1 ratio for 1h. Uncleared apoptotic cells were removed, and macrophages were either analyzed via flow cytometry (First Corpse, Left) or rested for 1.5h. Rested macrophages were then cultured with CypHer5E-labeled apoptotic MDA-MB-231 cells at a 1:1 ratio for 1h and analyzed via flow cytometry (Second Corpse, Right). Data represent three independent experiments. Data are shown as mean ± SEM. ***p < .001; ****p < .0001; ns = not significant.

(D) Time-lapse microscopy analysis of continual efferocytosis in chronic hypoxia-conditioned macrophages with disrupted PPP metabolism. Experiments were performed as in **Figure 1E and 1F** with the inclusion of 6-AN and vehicle control treatment conditions. Shown are representative images (Left), quantification of the number of CypHer5E+ events (Top Right), and analysis of the rate of apoptotic cell degradation (Bottom Right). For quantification, 53 efferocytotic macrophages from 5 vehicle-treated chronic hypoxia scenes and 51 efferocytotic macrophages from 7 6-AN-treated chronic hypoxia scenes were analyzed. Data were binned as number of events per cell and presented as a fraction of 100%. For analysis of degradation rate, 21 (vehicle-treated) and 13 (6-AN-treated) efferocytotic macrophages were analyzed. Time to degradation was defined as the time it takes to shrink an internalized corpse 50% after initial acidification (CypHer5E+). Data shown as mean ± SEM. ****p < .0001

(E) Perturbation of PPP metabolism reduces NADPH production in chronic hypoxia-conditioned macrophages. Macrophages were differentiated and conditioned as in **Figure 6B**. Indicated treatments (or vehicle controls) were added prior to the start of an assays. $NADP^+$ and NADPH relative luminescence units were detected using a plate reader. Data are from three independent experiments. Data are plotted as the ratio of $NADP^+$ to NADPH and presented as mean ± SEM. *p < .05; **p < .01.

(F) Chronic hypoxia-conditioned macrophages consume PPP-dependent NADPH during efferocytosis. Macrophages were differentiated and conditioned as in **Figure 6B**. Conditioned macrophages were cultured with apoptotic MDA-MB-231 cells at a 1:1 ratio for 1h. Uncleared

apoptotic cells were removed, and macrophages were lysed using a basic solution (0.2N NaOH, 1% DTAB) in a hypoxia chamber set to 1% O_2. $NADP^+$ and NADPH relative luminescence units were detected using a plate reader. Data are from three independent experiments. Data are plotted as the ratio of $NADP^+$ to NADPH and presented as mean ± SEM. **p < .01; ***p < .001; ****p < .0001.

(G) Lysosomal acidity increases in chronic hypoxia-conditioned efferocytotic macrophages with disrupted PPP metabolism. Macrophages were differentiated and conditioned as in **Figure 6B**. Conditioned macrophages were cultured with CypHer5E$^+$-labeled apoptotic MDA-MB-231 cells at a 1:1 ratio for 1h. Uncleared apoptotic cells were removed, and macrophages were stained with Lysosensor Green DND-189. CypHer5E$^+$ macrophages were gated as actively efferocytotic for analysis of lysosomal acidification. Shown are representative FACS plots (Left) and MFI (Right) from three independent experiments per condition. Data are shown as mean ± SEM. *p < .05; ****p < .0001.

(H) Lipid peroxidation increases in chronic hypoxia-conditioned efferocytotic macrophages with disrupted PPP metabolism. Macrophages were differentiated and conditioned as in **Figure 6B**. Conditioned macrophages were cultured with CypHer5E$^+$-labeled apoptotic MDA-MB-231 cells at a 1:1 ratio for 1h. Uncleared apoptotic cells were removed, and macrophages were stained with C11-BODIPY 581/591. CypHer5E$^+$ macrophages were gated as actively efferocytotic for analysis of lipid peroxidation. Shown are representative FACS plots (Left) and MFI (Right) from three independent experiments per condition. Data are shown as mean ± SEM. *p < .05; ***p < .001; ****p < .0001.

(I) Cellular ROS increases in chronic hypoxia-conditioned efferocytotic macrophages with disrupted PPP. Macrophages were differentiated and conditioned as in **Figure 6B**. Conditioned macrophages were cultured with CypHer5E$^+$-labeled apoptotic MDA-MB-231 cells at a 1:1 ratio for 1h. Uncleared apoptotic cells were removed, and macrophages were stained with CellRox Deep Red. CypHer5E$^+$ macrophages were gated as actively efferocytotic for analysis of cellular ROS. Shown are representative FACS plots (Left) and MFI (Right) from three independent experiments per condition. Data are shown as mean ± SEM. **p < .01; ****p < .0001.

Figure 6: Noncanonical pentose phosphate loop supports continual efferocytosis

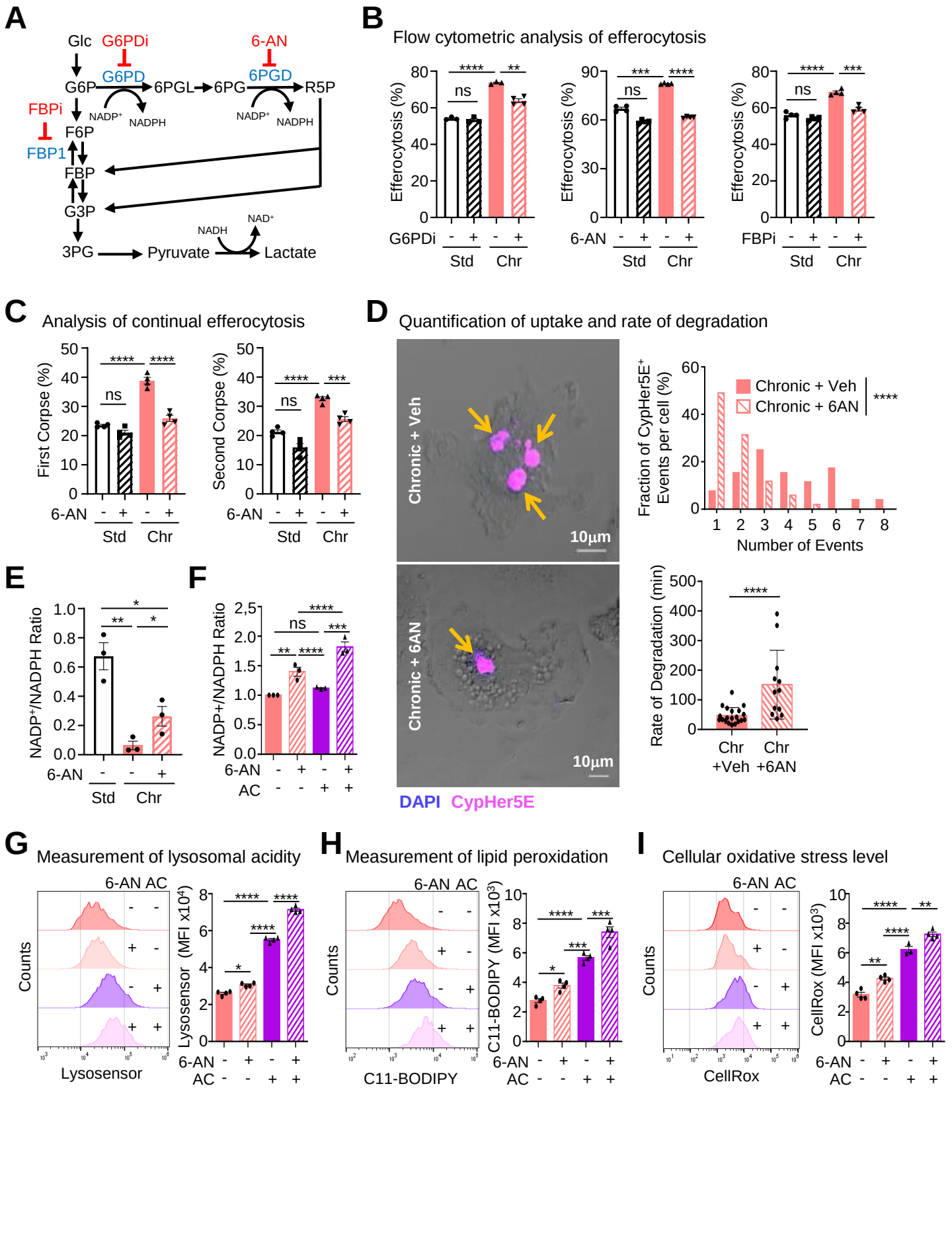

Figure 7: Perturbation of the pentose phosphate pathway impedes breast cancer progression

(A) Measurement of tumor volume in mice treated with 6-AN or vehicle. E0771 breast cancer cells were orthotopically implanted into the 4^{th} mammary fat pad of adult female C57BL/6J mice. Treatment was initiated at the first sign of palpable tumor and was performed as indicated. Tumor volume was measured using a caliper. Shown is the tumor volume relative to day 6 (Left) and the day 23 tumor volume. Both vehicle and 6-AN conditions included n=4 mice. Data are shown as mean ± SEM. **p < .01; ****p < .0001.

(B) Analysis of macrophage subsets in tumor-bearing mice treated with 6-AN or vehicle. Shown are the frequencies of macrophage subsets identified in tumors from **Figure 7A**, as defined by level of co-expression of F4/80 and CD11b in $CD45^{+}CD3^{-}TCR\beta^{-}$ cells. Data are shown as mean ± SEM. ***p< .001; ****p < .0001; ns = not significant.

(C) $CD8^{+}$ T cells increase in 6-AN-treated tumor-bearing mice. Shown are the frequencies of $CD8^{+}$ (Left) and $CD4^{+}$ (Right) T cells as a fraction of $CD45^{+}CD3^{+}TCR\beta^{+}$ cells in tumors from **Figure 7A**. Data are shown as mean ± SEM. **p < .01; ns = not significant.

(D) PPP metabolism disruption reverses macrophage phenotype in tumor-bearing mice. Macrophage subsets identified in **Figure 7B** were analyzed for co-expression of MHCII and Arginase 1 (Arg1). Shown are the frequencies of one of four subsets defined by MHCII and Arg1 expression and presented as a fraction of the indicated macrophage subset (e.g., $F4/80^{high}CD11b^{high}$ or $F4/80^{inter}CD11b^{high}$ macrophages). Data are shown as mean ± SEM. *p < .05; **p < .01; ***p < .001; ns = not significant.

(E) Perturbation of PPP metabolism impairs efferocytosis in tumors *in vivo*. Sections of tumors from Figure 7A were analyzed for the presence of secondary (uncleared) apoptotic cells using the terminal deoxynucleotidyl transferase dUTP nick-end labeling (TUNEL) assay. Entire slides were imaged via 63x slide scanner. Regions featuring at least one TUNEL+ Hoechst+ cell were used for analysis, which resulted in 26 regions for vehicle-treated tumors and 21 regions for 6-AN-treated tumors. Shown are representative images of the lower- and upper-bounds of TUNEL-positivity for both vehicle-treated and 6-AN-treated tumors (Left) and summary data (Right). Data are shown as mean ± SEM. ****p < .0001.

Figure 7: Perturbation of the pentose phosphate pathway impedes breast cancer progression

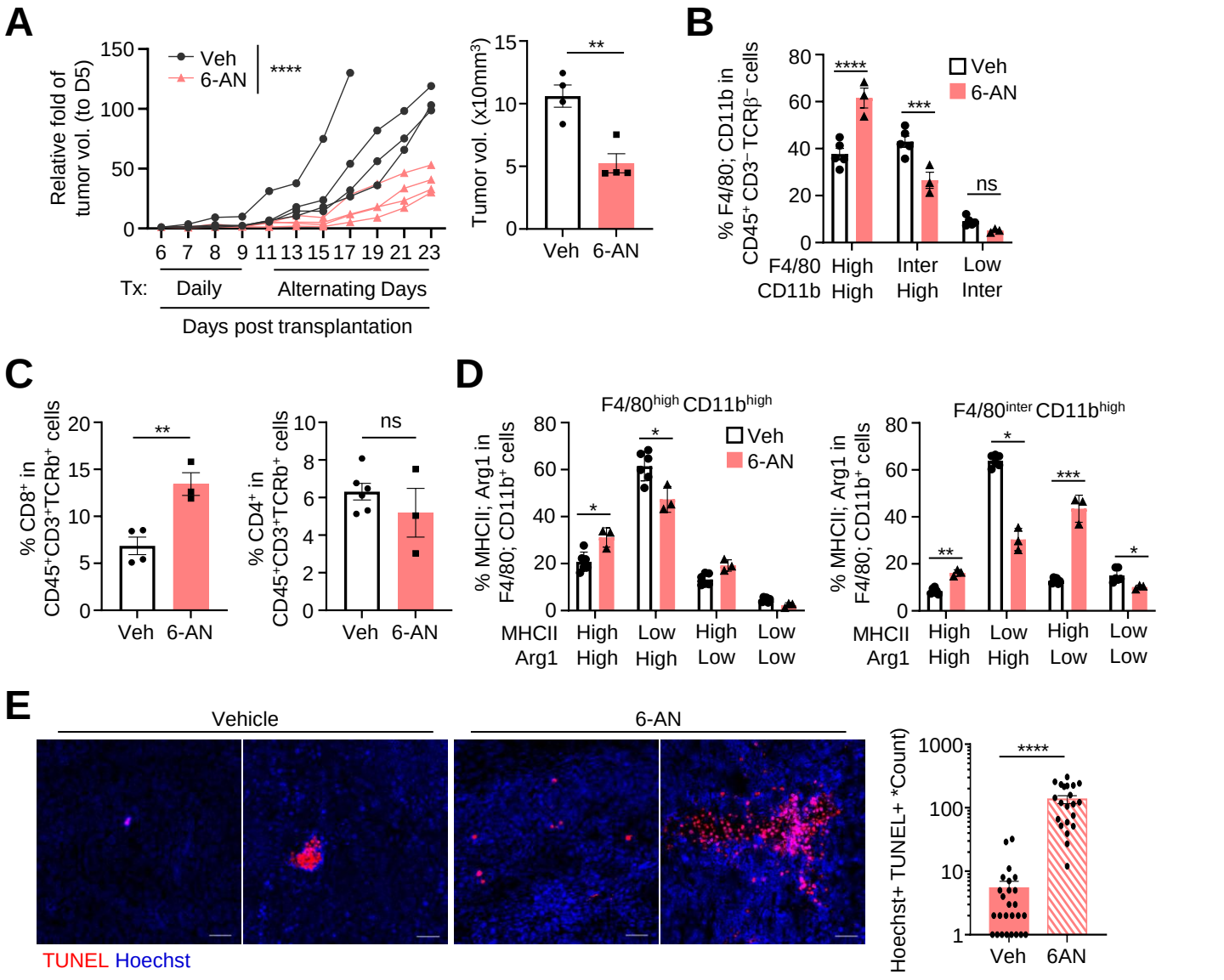

Figure S7: Perturbation of the pentose phosphate pathway impedes breast cancer progression

(A) Body weights tumor-bearing mice treated with 6-AN or vehicle. Shown are body weight measurements of mice bearing E0771 tumors from **Figure 7A**.

(B) Gating strategy of analyses in Figure 7B and 7C. Shown are representative FACS plots illustrating the gating strategy used to subset macrophages and analyze MHCII and Arg1 expression.

(C) No change in NK cells or regulatory T cells in 6-AN-treated tumor-bearing mice. Shown are the frequencies of $NK1.1^{+}$ NK cells as a percentage of $CD45^{+}CD3^{-}TCR\beta^{-}$ cells (Left) and $Foxp3^{+}$ regulatory T cells as a fraction of $CD45^{+}CD3^{+}TCR\beta^{+}$ cells (Right) in tumors from **Figure 7A**. Data are shown as mean ± SEM. ns = not significant.

Figure S7: Perturbation of the pentose phosphate pathway impairs breast cancer progression